Universiteit Utrecht

# Noble metal promotion for $Co/TiO_2$ Fischer-Tropsch catalysts

Thesis for the degree of Master of Science

Masterprogramme: Nanomaterials: Chemistry & Physics


Jogchum Oenema BSc

Supervisors:

Dipl. Chem. Thomas O. Eschemann MSc

Prof. Dr. Ir. Krijn P. de Jong

Utrecht University


January, 2015

# Table of contents

# List of figures

# List of abbreviations

| | |
|---|---|
| ATR | Autothermal Reforming |
| BET | Brunauer–Emmett–Teller |
| $C_{5+}$ | Hydrocarbons consisting of a chain of five or more consecutive carbon atoms |
| CPOX | Catalytic Partial Oxidation |
| CTY | Cobalt Time Yield |
| FID | Flame Ionization Detector |
| FT | Fischer-Tropsch |
| FTO | Fischer-Tropsch to Olefins |
| FTS | Fischer-Tropsch Synthesis, mostly used to refer to high alpha FT synthesis |
| GC | Gas Chromatography |
| GHSV | Gas Hourly Space Velocity |
| HP | High Pressure |
| HT | High Temperature |
| LP | Low Pressure |
| LT | Low Temperature |
| NG | Natural Gas |
| POX | Partial Oxidation |
| $S_n$ | Selectivity of a reaction to a certain product with n consecutive carbon atoms |
| SSITKA | Steady State Isotopic Transient Kinetic Analysis |
| SMR | Steam Methane Reforming |
| STY | Site Time Yield |
| TCD | Thermal Conductivity Detector |
| TEM | Transmission Electron Microscopy |
| TOF | Turn Over Frequency |
| TON | Turn Over Number |
| TPR | Temperature Programmed Reduction |
| WGS | Water-Gas Shift |
| WHSV | Wheight Hourly Space Velocity |
| WTY | Weight Time Yield |
| XRD | X-Ray Diffraction |

# 1. Introduction

## 1.1 Introduction and history of the Fischer-Tropsch process

The Fischer-Tropsch synthesis (FTS) describes the catalytic conversion of syngas (mixture of CO and $H_2$) into hydrocarbons. Syngas can be derived from a variety of feedstocks like: natural gas, coal and biomass. Generally, the synthesized hydrocarbons are further processed to ultra-clean fuels, lubricants or used as building blocks for polymers. The FTS is a widely and intensively studied topic in chemical research starting from its discovery in 1923 to the present day.[1]

The first experiments on catalytic hydrogenation of carbon monoxide were carried out by Sabatier and Senderens in 1902. From a mixture of CO and/or $CO_2$ with $H_2$ on cobalt or nickel catalysts, methane could be synthesized. This reaction took place at a temperature of 180-200˚C and at a pressure of 1 bar.[2–4] Continuing on these results, Mittasch and Schneider discovered that from mixtures of CO and $H_2$ in the presence of a supported metal catalyst hydrocarbon chains could be synthesized. They reported activity on several metals and metal oxides, such as supported cobalt oxide.[5–8]

Further progress was made by Franz Fischer and Hans Tropsch at the Kaiser Wilhelm Institut für Kohlenforschung in Mulheim, currently known as the Max Planck institute for Coal Research. Both researchers studied CO hydrogenation on iron and cobalt. In 1922 they proposed the Synthol process which produced a mixture of aliphatic oxygenated compounds via reaction of CO with $H_2$.[9–12] The reaction was performed at a temperature of 673 K and at a high pressure of >100 bar with alkalized iron chips as catalyst. Synthol was transformed after heating under pressure into “Synthine”, a mixture of hydrocarbons. In 1923 an important discovery was made: by lowering of the synthesis pressure to ~7 bar, heavy hydrocarbons could be produced on Fe/ZnO and $Co/Cr_2O_3$ catalyst. Franz Fischer and Hans Tropsch patented this process in 1925 and in 1926 their discovery was reported in literature and used in a pilot plant in Germany.[1,11,13]

In 1927, Roelen and his team at Ruhrchemie AG proposed chemical engineering solutions for applying FT synthesis as an industrial process. As a result the first large-scale FT plant, based on brown coal, operated in April 1936 as can be seen in figure 1a. The catalyst being used was cobalt promoted with thorium and supported on kieselguhr. Kieselguhr is also known as diatomaceous earth, and is a naturally occurring microporous material consisting of silicate and small amounts of alumina and iron oxide.[14] Soon afterwards more German FT plants were built; in 1939 nine FT plants were operational in Germany with a combined capacity of 740,000 metric tons of primary products per year.[1,16]

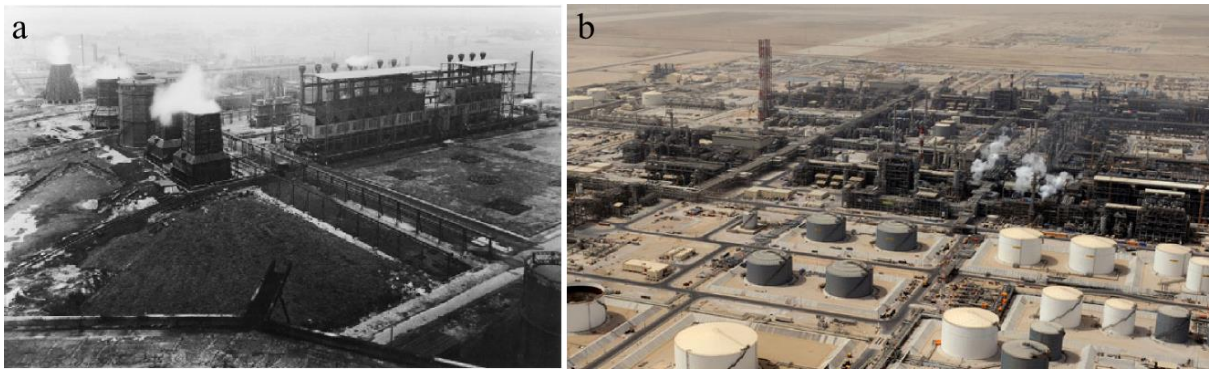


**Figure 1: a: Ruhrchemie AG FT production plant in Oberhausen, Germany in 1936. b: Shell pearl GTL in Las Raffan, Quatar in 2011.**[17,18]

The synthesis of FT fuels reached a peak in 1944 during the Second World War when German supplies of fossil fuel resources were cut off by the allied forces and the German factories were turning out 570,000 metric tons per year. The feedstock for the FT process was mainly domestic (brown) coal and to a small extent other materials.[15,18]

After the Second World War the process remained popular because it was expected that the crude oil reserves were quickly diminishing. New FT plants were built in Brownsville, Texas in 1950 and in South-Africa in 1955. However, the availability of crude oil increased tremendously in the mid-1960s by advances in drilling and the discovery of new oil wells in the Middle East causing a decreased popularity of the process in Europe and America. As a consequence, the remaining FT plants in Europe and America were no longer profitable and were closed and dismantled. An exception is South-Africa, where the coal based FT process was still being used in this period. South-Africa has a large availability of domestic coal which can be used as a cheap feedstock. Furthermore, on 20 November 1987 the United Nations General Assembly adopted an international oil embargo on South-Africa to put pressure on the South-African government to end the racist policies of apartheid. As a reaction to the embargo, the South-African government pursued to be independent from foreign supplies of crude oil.[1,21,22]

From the 1980s until now, various drivers cause an renewed interest in the FT process; major petroleum companies re-initiated research in the FTS and related development programs.[1] The most important driver is the increasing worldwide demand for (liquid) fuels, caused by an increasing worldwide energy demand.[23] Gasoline or diesel sold nowadays in Europe consists of a mixture of hydrocarbon products derived from different feedstocks, e.g.: 97% crude oil and 3% other sources such as bioethanol or Gas to liquids (GTL) fuel.[24] The price of these liquid fuels is therefore highly dependent on the price of crude oil which is very volatile as can be seen in graph 2. Different events in the last century caused drastic changes in the availability and demand and therefore in the price of crude oil. The FT process can act as an alternative and/or supplementary way for using different carbon feedstocks to obtain liquid fuels, independent of the availability of crude oil. The Shell GTL process is estimated to breakeven with petrol derived from crude oil at a price of $ 36 per barrel, whereas Coal to liquids (CTL) breaks even at $ 60 and Biomass to liquids (BTL) at $ 75.[25]

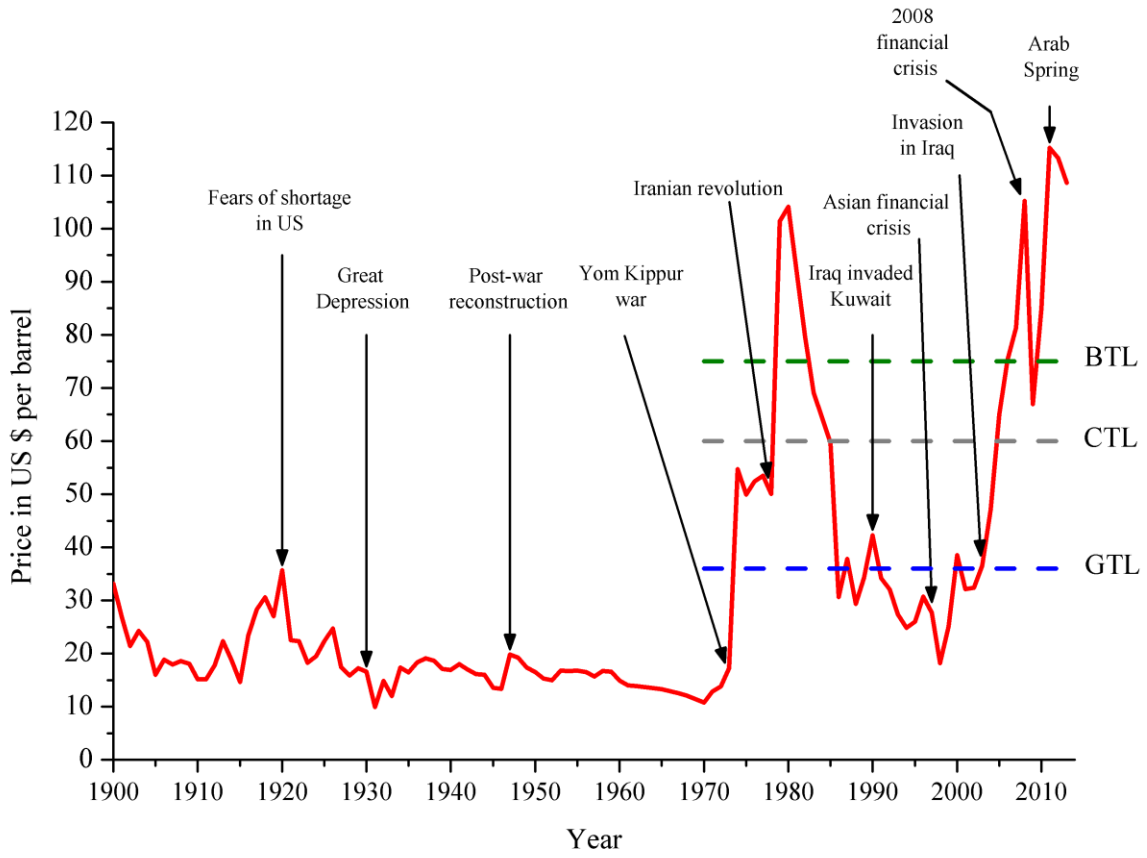


**Figure 2: Average annual oil price from 1900 to 2013 corrected for inflation in 2013. The horizontal lines represent the break-even points of Biomass to liquids, Coal to liquids and Gas to liquids.**[23,25]

**Table 1: Summary of the global reserves of crude oil, natural gas and coal. The results are estimated values, including unconventional feedstocks (e.g.: tight oil, shale gas and oil derived from tar sands) which can be recovered, with reasonable certainty, from known reservoirs in the future under existing economic and operating conditions.** [23,26,27]

| | Crude oil reserve in barrels ($\times 10^9$) | Natural Gas reserve in barrel equiv. ($\times 10^9$)[1] | Coal reserve in barrel equiv. ($\times 10^9$)[2] |
|---|---|---|---|
| North America | 230 | 77 | 875 |
| South & Central America | 330 | 51 | 54 |
| Europe & Eurasia | 148 | 374 | 985 |
| Middle East | 809 | 530 | 5 |
| Africa | 130 | 94 | 155 |
| Asia Pacific | 42 | 100 | 1.090 |
| World | 1.687 | 1.226 | 3.163 |
| Global yearly consumption[3] | 33 (2.0 % of total reserve) | 22 (1.8 % of total reserve) | 28 (0.9 % of total reserve) |
| ERI by conversion to fuel[4] | 0.80 | 0.54 (Shell GTL) | 0.27 (Sasol CTL) |

[1] The conversion to barrel equivalent was based on calorific values after refining.

[2] The conversion to barrel equivalent was based on calorific values after refining.

[3] The consumption was the global yearly consumption in 2013.

[4] The energy return on investment (ERI) is an index number obtained by comparing the initial energy value of the feedstock and the energy value of the final product. This index number gives an idea of the energy efficiency of the process.

The depletion of the worldwide crude oil reserves is another driver for an increased interest in the FT process. In table 1 has been tried to give an overview of the current situation of the world reserves of fossil fuels. Assuming a constant demand, the currently know reserves for crude oil and natural gas are enough for approximately 50 years. However, in the last decade (2003-2013), the demands for crude oil and natural gas have increased by respectively 14 % and 29 % and will most likely continue to increase in the near future. On the other hand, new oil wells and gas fields are continuously being discovered making it hard to make good predictions of the exact crude oil reserves.[23]

A number of remote gas fields discovered in the last decades are considered as 'stranded', because it is not economically viable to recover the gas from the field entailing the need for a costly pipeline infrastructure. Stranded gas is also frequently found as side product from oil drilling and is often flared at the drilling site. In order to reduce the global greenhouse gas emissions, the Worldbank encourages countries to utilize the flared gas and thereby making oil drilling more efficient. In 2005, 172 billion cubic meters of natural gas (1,1 billion barrel equiv.) was flared whereas in 2010 the amount decreased to 134 billion cubic meters (0,9 billion barrel equiv.), mainly caused by investments in gas utilisation projects in Russia and Kazachstan.[26] The FT process (on a small scale) can allow the utilization of stranded gas by converting natural gas on-site into hydrocarbon liquids having a higher specific energy than natural gas and are therefore economically viable to be transported in a ship or truck.[21]

By using FTS non fossil, biomass based feedstocks can be converted into useful products and materials. By catalytic partial oxidation of biomass syngas with a low $H_2$/CO ratio and a high concentration of impurities can be obtained. By using supported iron catalysts, short unsaturated hydrocarbons are synthesized used for polymer production. A side product of this process are longer parrafins which can be used as fuels. This process is also often reffered to as Fischer-Tropsch to Olefins (FTO).[28,29]

The possibility to produce ultra-clean automotive fuels is another incentive for FTS. Ultra-clean fuels are required to meet the demands on increasingly stringent environmental legislation. Fuel derived from crude oil often contains contaminations like: sulfur species, aromatics and hetero-atom aromatics. Ultra clean fuel from the FT process can be mixed with fuel derived from crude oil to reduce the emission sulfur oxides, and by more efficient combustion properties also the emissions of particulate matter and carbon monoxide can be reduced.[29,30]

Another driver is the possibility to synthesize large hydrocarbons which can be used directly as specialty chemicals or are further converted into products such as lubricants. Specialty chemicals have a higher profit margin than fuel and can therefore be used to increase the profit from a FT plant. After the peak in the oil prices in the 1980's the oil price decreased sharply and was low for approximately 20 years. The FT plants operating in that period could be made profitable by synthesizing specialty chemicals.[31]

## 1.2. Syngas production

The $H_2$/CO ratio and purity of the syngas depends, among other factors, on the feedstock. Large scale syngas production from natural gas can be performed by: steam reforming (SMR), autothermal reforming (ATR) or partial oxidation (POX). SMR is an energy intensive reaction which takes place at 700-900 ˚C and elevated pressures using a nickel catalyst. The energy for this reaction is usually obtained by the heat generated from the FTS, the energy from the water-gas shift side reaction and by using $H_2$ from the product stream. POX is the direct oxidation of methane with oxygen to CO forming two stoichiometric amounts of $H_2$. It can be carried out at 1100˚C (Thermal POX) or at 700˚C using a

noble metal catalyst (Catalytic POX). Partial oxidation of methane is not evident, it is essential that the contact time of the methane-oxygen mixture with the catalyst is in the millisecond range.[29] The relevant reactions equations with their corresponding energy values are shown here:

Steam methane reforming: $CH_4 + H_2O \rightleftarrows 3\,H_2 + CO$ $\Delta H° = +206$ kJ·mol$^{-1}$ (1)

Partial oxidation: $CH_4 + \frac{1}{2}\,O_2 \rightleftarrows 2\,H_2 + CO$ $\Delta H° = -36$ kJ·mol$^{-1}$ (2)

Another way to produce syngas is ATR, which is a combination of SMR and POX. The reaction mixture of ATR is self-reliant on energy implying that no external energy is needed. In the larger FT plants in Bintulu, Malaysia and Ras Laffan, Qatar owned by Shell non catalytic partial oxidation is used to produce syngas.[31] Syngas made from natural gas has a $H_2$/CO ratio of ~2 and a low concentration of impurities making it suitable for cobalt based FTS. Cobalt particles are more active and are more resistant to synthesis gas with a high $H_2$/CO ratio compared to e.g. iron.[32]

## 1.3. Fischer-Tropsch synthesis

### 1.3.1. Fischer-Tropsch reactions

During FTS hydrocarbons of different length and structure are formed of synthesis gas by surface polymerization on a metal catalyst. The prevailing reactions during synthesis are:

n-alkanes: $n\,CO + (2n+1)\,H_2 \rightleftarrows C_nH_{(2n+2)} + n\,H_2O$ $\Delta H° = -165$ kJ·mol$^{-1}$ (3)

α-alkenes: $n\,CO + 2n\,H_2 \rightleftarrows C_nH_{(2n)} + n\,H_2O$ $\Delta H° = -165$ kJ·mol$^{-1}$ (4)

These reactions are highly exothermic: the formation of one mole of the building block $CH_2$ generates 165 kJ.[28] The main product formed during cobalt based FTS at high pressures are $C_{5+}$ alkanes. The range of $C_5$-$C_{16}$ hydrocarbons is in the form of liquids while $C_{16+}$ hydrocarbons are in the form of wax at room temperature. The main side products are methane and short α-alkenes which are usually in the $C_2$-$C_6$ range. Other products can be formed when hydrogenation or isomerization sites are present on the cobalt particles. Cobalt catalyzed FTS is performed industrially between 200-250°C and at 20 bar.[29]

Water is the main stoichiometric product formed during FTS. Water can react via the water-gas shift reaction (WGS) with CO to form $CO_2$ and $H_2$.

Water-gas shift reaction: $CO + H_2O \rightleftarrows CO_2 + H_2$ $\Delta H° = -41$ kJ·mol$^{-1}$ (5)

When the WGS is significant during FT it causes a higher $H_2$/CO ratio which reduces the chain growth probability and therefore increases the selectivity towards short hydrocarbon chains. The negative effects of the WGS are mainly noticeable in iron based FTO and to a lower extent in cobalt based FTS. To avoid the negative effects it is important to find a compromise between CO conversion and water-gas shift during FTS.[29,33]

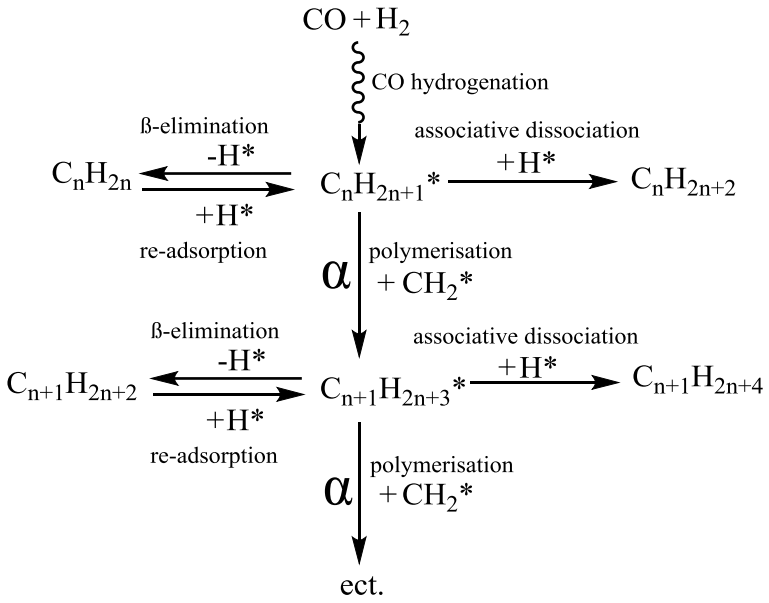


**Figure 3: Schematic representation of FT chain growth.**[21,31,34,35]

While the exact mechanism of the FTS is still under debate, a widely accepted model for chain growth states that carbon chains are synthesized by surface polymerization of methylene groups ($CH_2$).[21,31,34,35] As can be seen in figure 3, methylene groups are synthesized by CO hydrogenation and can migrate over the surface to polymerize with adsorbed alkyl groups adding a carbon atom to the alkyl chain. The probability of polymerization during FTS is referred to as α. Termination of chain growth can either occur via β-elimination to form an $\alpha$-alkene, or dissociation to form an n-alkane. β-hydrogen abstraction is a reversible chain termination step at typical FTS conditions. Re-adsorption of α-olefins leads to the re-initiation of alkyl surface chains and possibly to the formation of larger hydrocarbons. The probability of chain growth termination via either routes is (1-α).

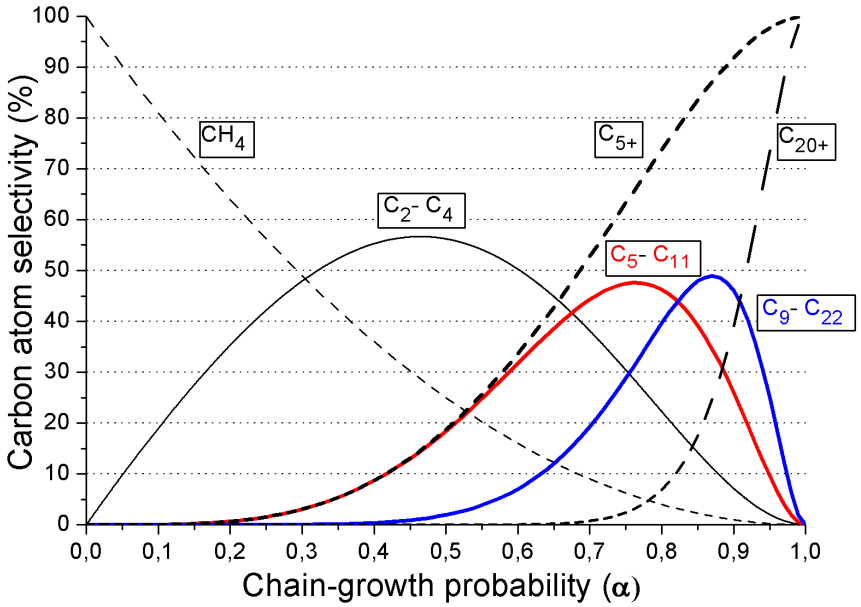


**Figure 4: The carbon atom selectivity correlates directly to the chain-growth probability.**[27]

The α of a reaction is an important factor determining the product selectivity as can be seen in figure 4. The α depends on process conditions such as: temperature, pressure, gas hourly space velocity

(GHSV) and the catalyst that is used. High temperatures and high $H_2$/CO ratios favor termination, resulting in a lower α, whereas low $H_2$/CO ratios increase the selectivity toward olefins. Very high chain-growth probabilities are regarded desirable as they lead to reasonable primary selectivity's to fuel ranges and high selectivities to heavy components, which subsequently can be converted to liquid fuels using conventional refinery technologies.[31,34,35]

### 1.3.2. Industrial Fischer-Tropsch reactors

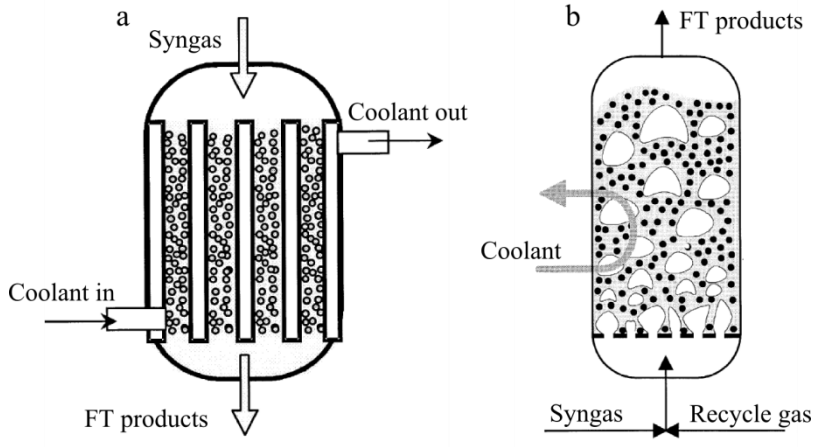


**Figure 5: FT reactors used in industry a: Multi tubular reactor for heavy paraffin or middle distillate synthesis used, among others, by Shell. b: bubbling fluidized bed reactor used by Sasol in the Synthol process. Images reproduced from [35].**

FTS in industry takes place in large chemical reactors which exist in a variety of types with either a fixed catalysts bed or a moving catalyst bed. The two most relevant reactors are the Multi tubular reactor and the Bubbling fluized bed reactor which both can be seen in figure 5. Multi-tubular fixed-bed reactors were developed by Lurgi GmbH and Ruhrchemie A.G. and are nowadays used in the Shell middle distillate synthesis (SMDS). The syngas enters the reactor from above and flows through small diameter tubes with catalyst material. The tubes are surrounded by a heat exchanger filled with water to create enough heat-removal capacity. The catalyst consists of pellets or extrudates which size is optimized to minimize diffusion limitation and pressure drops over the reactor. In a bubbling fluidized bed reactor the reactant stream enters from underneath and is bubbled through a slurry of long chain hydrocarbon liquid products and catalyst particles. Unreacted synthesis gas and light products leave the reactor in the gas phase, while the liquid products are removed as a part of the slurry. Heat is removed by cooling coils mounted inside the reactor. This type of reactor is mainly used by Sasol in the Synthol process. An overview of all large FT plants worldwide and their reactors is given in table 2. [27,34,35]

**Table 2: Overview of the properties and of large FT plants worldwide. Data reproduced from:[27,36].**

| Company | Location | Start-up date | Carbon feedstock | Catalyst type | Reactor type | Approx. capacity (barrels/day) |
|---|---|---|---|---|---|---|
| Sasol | Secunda, South Africa | 1980/ 1995 | Coal & NG | Fe/K | HTFT circulating fluidized bed | 160.000 |
| Shell | Bintulu, Malaysia | 1992 | NG | $Co/SiO_2$ $Co/TiO_2$ | LTFT multitubular fixed bed | 14.500 |
| PetroSA | Mosselbay, South Africa | 1993 | NG | Fe/K | HTFT circulating fluidized bed | 22.000 |
| Sasol-QP (Oryx) | Ras Laffan, Qatar | 2007 | NG | $Co/Al_2O_3$ | LTFT slurry phase | 34.000 |
| Shell (Pearl) | Ras Laffan, Qatar | 2011 | NG | $Co/TiO_2$ | LTFT multitubular fixed bed | 140.000 |
| Chevron-Sasol | Escravos, Nigeria | 2014 | NG | $Co/Al_2O_3$ | LTFT slurry phase | 120.000 |

### 1.3.3. Heat transfer during FTS

For optimal FTS, there should be a homogeneous distribution of temperature and reactants through the reactor. FTS is a highly exothermic reaction as can be seen from equations 2.3 and 2.4, making it essential to have a high heat removal capacity in the reactor. In liquid-solid mode the heat of reaction is removed by liquid hydrocarbons of the product stream. In gas-solid mode the heat removal capacity can be low caused by the low heat conductivity of the gaseous phase leading to temperature gradients in the reactor. Since the heat release during FT is proportional to the reaction rate, the heat transfer problems mainly occur at locations in the catalyst bed where most CO and $H_2$ are converted. If the conversion is high on a certain place on the catalyst bed, for instance at a region that contains a high amount active sites, hotspots can occur. In a hotspot the temperature is significantly higher than in the rest of the catalyst bed, which might accelerate catalyst degeneration. To prevent temperature gradients in the catalyst bed, the catalyst is usually mixed with diluent particles which is are inert, non-porous and heat resistant. [1,35]

## 1.4. Fischer-Tropsch catalysts

### 1.4.1. Composition of a Fischer-Tropsch catalyst

A typical industrial catalyst for cobalt based FT consists of at least four different components:

- Cobalt as the **active metal** (8-30 wt.%)
- **Support** which is usually a refractory metal oxide
- **Reduction promoter** which is usually a noble metal (0.05-1 wt.%)
- **Structural promoter** which is usually a metal oxide (1-10 wt.%)

The role of the active metal and support will be explained in the following sections. The reductional and structural effects of noble metals as promoter will be discussed in chapter 2. Metal oxides acting as structural promoters which help to maintain cobalt dispersion during catalysis (e.g.: $ZrO_2$, $SiO_2$ and $La_2O_3$) are beyond the scope of this project and will therefore not be discussed.[27]

### 1.4.2. Metals with activity in the Fischer-Tropsch reaction

In the choice of the catalytic metal a number of aspects are important: activity, selectivity, cost and abundance of the metal in nature. Most metals of groups 8-10 of the periodic table have noticeable activity in the hydrogenation of CO. Franz Fischer was the first to research the activity of different group VIII metals in the methanation reaction. Fischer used unsupported metals and normalized the conversion on the weight of the catalyst he used. The results he obtained were of great importance to the further development of the FT catalysts. More recently, Vannice et al. reported the activity of group 8-10 metals, using $Al_2O_3$ as support and using the specific activity of the catalyst expressed as the turn over frequency. The turn-over frequency of the FT reaction is most often defined as the number of CO molecules converted per active site per second.[37,38] The amount of active sites was derived from the metal surface area obtained from $H_2$-chemisorption experiments. The results of Vannice are displayed in table 3, but it should be noted that not all metals in the table are suitable as FT catalysts on industrial scale. Ruthenium and rhodium are too scarce and expensive, while nickel, palladium and platinum (group 10) are highly selective for methane. Therefore, iron and cobalt are the most suitable metals for FTS on an industrial scale. Iron is roughly twenty-five times cheaper than cobalt and is more resistant to poisons in the product stream. However, disadvantages of iron are fast deactivation of both activity and selectivity and a profound effect of the water-gas shift effect at high conversions. In table 2 can be seen which active metal is used in large scale FT plants.[1,28,32]

**Table 3: Summary of the activities and selectivities of different metals. The catalytic tests of Vannice were conducted at 1 atmosphere and at 240 °C. The difference in results can be attributed to the method of determining the activity, particle size effects and metal support interactions.[37,38]**

| | Specific activity turn over number ($\times 10^{-3}$) |
|---|---|
| Ruthenium | 181 |
| Iron | 57 |
| Nickel | 32 |
| Cobalt | 20 |
| Rhodium | 13 |
| Palladium | 12 |
| Platinum | 2.7 |
| Iridium | 1.8 |

### 1.4.3. Support used for FT catalysts

The catalytically active metal in industrial FTS is usually dispersed on a support. Using a support instead of bulk metals has numerous advantages: metal particles can be dispersed on the support resulting in a larger metal surface area per gram of metal. Furthermore the reduction properties of the active metal, such as reduction temperature and ease of reduction, are improved, and clustering of metal particles during reaction is prevented. By dispersion of metal particles on a support of a certain

sieve fraction pressure drops over the catalytic reactor are avoided. By increasing the metal surface area, the number of active sites per mole of cobalt increases. Most common support materials are metal oxides like $SiO_2$ and $Al_2O_3$ or $TiO_2$ as can also be seen in table 2. A support that is used in research is carbon, either in the form of carbon nanotubes or carbon nanofibers. The disadvantage of carbon is the high price making it unsuitable for use in industry.[39]

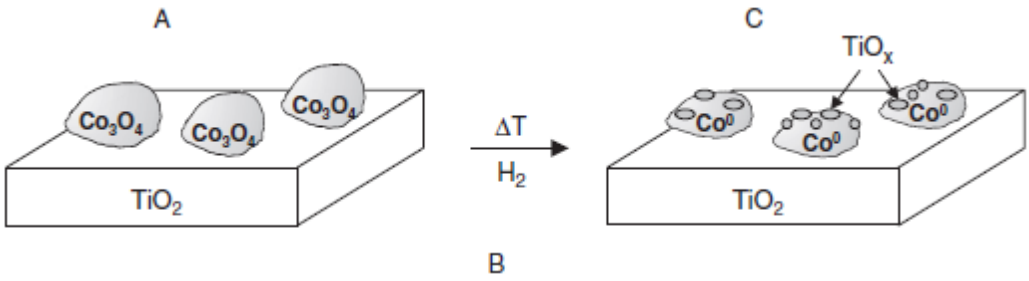


**Figure 6: A schematic representation of $TiO_2$ patches migrating on cobalt particles during reduction. Reproduced from:[22].**

A reducible support in combination with a catalytic metal can be partly reduced during a reduction causing so called strong metal support interactions. SMSI effects involve a number effects unseen for metals supported on an inert support. The most significant effect is the arise of mixed metal oxide patches migrating over the catalyst surface on metal cobalt particles. This effect is called $TiO_x$ or mixed oxide decoration. This partial encapsulation of the metal particle by the support oxide species can lead to a decrease in catalytic activity because the metallic surface area decreases and the mixed oxides are not active in FTS.

Another SMSI effect is the stronger binding between the catalytically active metal and the support, leading to different electronic properties of the metal. By XPS studies performed by Riva et al. was found that CoO could not be completely reduced on $TiO_2$ while it could be fully reduced as a bulk metal. This could be contributed to a higher binding energy between Co and Ti or due to the formation of a cobalt titanate.[41]

An advantage of $TiO_2$ is that it has a high hydrothermal stability and can withstand high water partial pressures. The rutile/anatase ratio can be tailored, which influences the surface area and mechanical properties. $TiO_2$ is a popular support for industrial applications as can be seen in Table . Cobalt particles supported on $TiO_2$ have a high selectivity for $C_{5+}$ products and have a good heat resistance.[28]

# 2. Noble metal promotion on $Co/TiO_2$ and other cobalt particle properties

## 2.1. Introduction

For FT catalysts in industry structural and reduction promoters are added as doping agents to improve their activity, selectivity and/or stability as has previously been discussed in section 1.4.1.[20] In this section the use and effects of noble metal promoters on $Co/TiO_2$ FT catalysts will be discussed. Furthermore, the different crystallographic phases of metallic cobalt and the cobalt particle size effect will be discussed.

## 2.2. Noble metals

Noble metal promoters have a number of effects on the performance of cobalt based FT catalyst, which can be divided in structural or electronic effects. Structural promoters affect the formation and stability of the active phase of a catalyst, whereas electronic promoters directly affect the elementary steps involved in each turnover on the catalyst.[20]

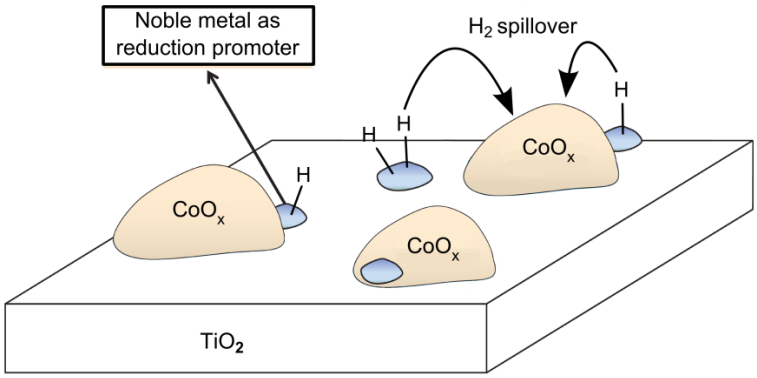


**Figure 7: Hydrogen spillover on the surface of a noble metal promoted $Co/TiO_2$ FT catalyst. The image was reproduced from [27]. (Image was modified afterwards).**

The most eminent structural effect of the addition of noble metal promoters is the decrease of the cobalt oxide reduction temperature. During a catalyst activation procedure using a reducing gas, noble metal oxides are reduced at low temperatures (100-200°C), while cobalt oxides reduce at (250-350°C).[41] However, a noble metal present on the catalyst support can facilitate the reduction of cobalt oxide by hydrogen spillover. When a $H_2$ molecule adsorbs on a noble metal particle, it forms mononuclear hydrogen which can migrate over the surface to cobalt oxide particles and thereby reducing cobalt oxide. The reduction of cobalt oxide at lower temperatures is therefore facilitated by the presence of noble metal species. A lower reduction temperature of a catalyst can reduce the energy costs of activation which can be of great importance when FT catalysts are applied on a large scale.[20,31]

Enhancement in cobalt dispersion is another structural effect due to introduction of noble metals to cobalt catalysts. A higher dispersion of cobalt particles were observed for catalysts promoted with rhenium, ruthenium, palladium and platinum.[1,20] A suggested reason for the higher cobalt dispersion could be related to a higher concentration of cobalt oxide nucleation sites during decomposition of cobalt precursors in the presence of promoting noble metals. A higher concentration of $Co_3O_4$ nucleation sites (at the same cobalt content) would result in a larger number of cobalt particles and consequently higher cobalt dispersion in the catalysts. Another reason responsible for the higher cobalt dispersion could be related to the lower temperature of reduction of cobalt species in the

presence of noble metals. Reduction at a lower temperature leads to a lower probability of formation of cobalt-support mixed oxides and/or sintering of the reduced cobalt metal particles, under the condition that the reduction is performed at a lower temperature. Schanke et al. showed that addition of platinum to $Co/SiO_2$ catalyst did not lead to a considerable increase in the extent of reduction. The total amount of chemisorbed $H_2$ after promotion with 0.4 wt.% Pt increased by more than 30%, while the extent of cobalt reduction was, respectively, 90% and 92% for unpromoted and platinum promoted cobalt catalysts. Higher FT reaction rates were attributed to an increase in cobalt dispersion due to the presence of platinum.[42]

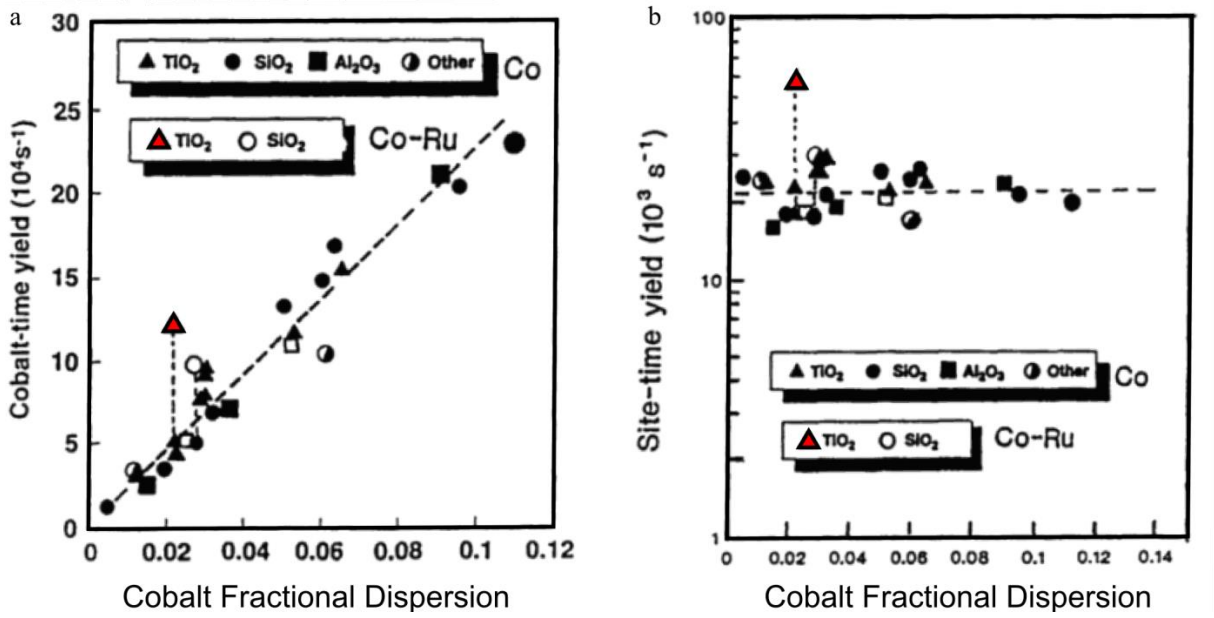


**Figure 4: a: The Cobalt time yield (CTY) plotted versus the cobalt fractional dispersion. b: The Site time yield (STY = TOF) plotted versus the cobalt fractional dispersion. The unpromoted catalyst have a TOF of $\pm 2.0 \cdot 10^{-3}$ $s^{-1}$, however the $Co/TiO_2$ promoted with Ru has a threefold higher TOF of: $5.3 \cdot 10^{-3}$ $s^{-1}$ (indicated with the red triangle). Reproduced from:[33] (modified).**

Another effect that can occur by noble metal promotion of cobalt FT catalyst with a reducible support is an increase of the TOF of the catalyst, caused by a synergistic effect between cobalt and the noble metal. Iglesia et al. reported such an bimetallic synergy for 11.3 wt.% Co on titania promoted with 0.14 wt.% Ru.[43] Arjan den Otter also found an increased TOF for cobalt supported on niobium and promoted with platinum.[44] Noble metals have usually a lower CO hydrogenation activity than cobalt, with the exception of ruthenium, as can be seen in table 3. However, together with cobalt it could result in a catalyst which is more active than the summation of the activities of both metals. Iglesia reported a threefold increased turn over frequency of $1.7 \cdot 10^{-3}$ $s^{-1}$ for the unpromoted catalyst, to $5.3 \cdot 10^{-3}$ $s^{-1}$ for the ruthenium promoted catalyst (Co/Ru = 0.0063 at.). The metal surface area of the catalysts was obtained by $H_2$ chemisorption and was used in combination with catalytic tests to determine TOF values. The explanation of Iglesia et al. for the increased TOF is the preservation of active sites during the reaction. The $H_2$ chemisorption experiments for the promoted and unpromoted catalyst yielded the metal surface area of fresh catalysts. However, during catalysis some active sites will get blocked, leading to a lower metal surface area and therefore lower number of active sites. Ruthenium atoms present on the surface of the catalyst, prevent blocking of active sites during catalysis by having a protective effect on the accessibility of reduced surface cobalt atoms, by either inhibiting of the oxidation of metallic cobalt atoms or preventing the deposition of carbon on active sites.[43] However, cobalt oxidation has been studied by A.M. Saib et al. who compared the results form literature in the period 2003-2009 and it was concluded that particles larger than 2 nm could not be

oxidized under FT conditions.[45] The prevention of carbon deposition during catalysis is however a realistic explanation of the observed results which would cause a significant increase in the apparent TOF.[45,46] Another explanation that can justify the increased activity to a very limited extent is catalytic activity of ruthenium. Small amounts of ruthenium present on the surface have a high activity for CO hydrogenation, as can be seen in table 3.

Storsæter et al. reported increased TOF for rhenium promoted Co catalyst supported on titania compared to unpromoted titania supported cobalt particles, both with similar cobalt dispersion.[47] The increased TOF is explained by the partly reduction of the support during the reduction due to SMSI. At low-temperature reduction this results in the formation of $TiO_x$ species. The $TiO_x$ species do not have enough mobility to achieve a significant transport over the metal, but they do have a promoting effect on the $CO/H_2$ reaction leading to a higher rate of CO dissociation and a higher TOF.

In literature it has been suggested that increased TOF values are caused by electronic promotion of the active site by the noble metal.[1] An electronic promoter directly affects the elementary steps involved in each turnover on an active site.[20] Noble metal promotion of cobalt catalysts can lead to bimetallic alloy formation. Alloys have a different local electronic structure caused by the addition or withdrawing of electron density from the cobalt atoms to or from neighboring noble metal atoms. Changes of the electron density take place in the valence band shifting the Fermi level. This results in a modification of the chemisorption properties of the catalyst and therefore the catalytic properties of the metal alter.[41]

The increased activity by noble metal promotion of cobalt on titania FT catalyst has not always been explained by bimetallic synergy or electronic promotion. Some studies report the increased activity of ruthenium promoted titania supported cobalt FT catalyst has been caused by an enhanced dispersion leading to a higher metal surface area, but not to a higher TOF.[48,49] While the fundamental explanation for the increase in TOF for titania supported catalysts is still under debate, there is a consensus in literature that for cobalt particles on irreducible supports a bimetallic synergy does not occur. Noble metal promoted cobalt on alumina FT catalyst have been researched and increased activities were reported for: platinum, palladium, rhenium and ruthenium.[41,43,50] The increases in activity could be fully explained by an increased metal surface area. Therefore noble metal promotion on alumina supported cobalt catalyst did not lead to a higher TOF. Similar results were found for a ruthenium promoted cobalt catalyst supported on silica.[43]

## 2.3. Particle size effect

The catalytic activity of catalytically active metal particles is dependent on the number of contact points of a reactant with the surface. The number of contact points depends on the arrangement of the surface atoms of the metal particles depending, amongst others, on the crystallographic structure and the size of the crystal.

Many researchers have studied the effect of the crystallite size of catalytically active metal particles on the arrangement of their surface atoms. Van Hardeveld et al. determined statistically that the average number of nearest neighbors of surface atoms of metal crystals are related to the size of a metal crystal under a certain particle size (<5 nm).[51] An apparent structure insensitivity of the catalytic reaction is expected above 5 nm, because the average ‘state’ (number and position of nearest neighbors) of surface atoms is not dependent on the size of the particle, assuming particles consist of perfect crystallites. To give an idea of the size of a typical active metal particle: the atomic radius of cobalt is 125 pm, which means that a spherical *fcc* particle with a diameter of 2 nm consist of roughly 2400 cobalt atoms.

To distinguish between types of active sites, sites are denoted as $B_n$, where n denotes the number of contact-points of a reactant with a site.[52] The type of $B_n$ sites present on a metal crystallite depends on which crystal planes are exposed at the surface. For CO dissociation,[53] $CH_x$ hydrogenation,[54] and C-C bond formation[55] on the surface of metal crystallites, the $B_5$ sites are the most active. For $B_5$ sites to be present the metallic particles should have a diameter larger than 2 nm and their surface should be 'rough', meaning that ridges are present with the 110 plane and the 113 plane exposed at the surface. When the particle is a perfect octahedron with only 111 and 100 planes exposed, only $B_3$ and $B_4$ sites are present.[52] Note however that (carbon induced) surface rearrangements during reaction are possible, changing the properties of specific active sites.[46,56]

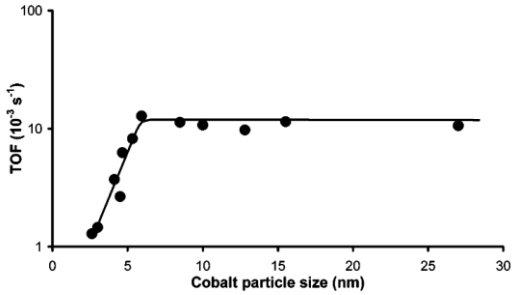


**Figure 8: Graph showing the effect of the cobalt particle size on the turn over frequency. Reproduced from.**[57]

Many researchers have reported a that the TOF on cobalt FT catalyst is independent of the cobalt particle size over a broad range.[33] G.L. Bezemer et al. published an experimental study about the effect of cobalt particle size on the TOF.[39] This experimental study was conducted using different cobalt catalyst with varying average particles sizes (2.6-27 nm) supported on functionalized carbon nanofibers.[58] A decrease in TOF was reported for particles below of 6 to 8 nm in size, as can been seen in figure 8. Furthermore, catalysts with an average particle size below 6 nm had higher methane selectivity's and (consequently) a lower $C_{5+}$ selectivity. In a follow-up article by Johan den Breejen et al. a longer $CH_x$ and $OH_x$ residence time and a shorter CO residence time for cobalt particles below 6 nm was reported.[37] The surface coverages of the $CH_x$, $OH_x$ and CO intermediates appeared to be constant for large particles. On the contrary, an increase in H coverage was observed for small (<6 nm) Co particles. From CO introduction experiments it was concluded that a significant amount of irreversibly bonded CO molecules is present on small particles too, causing blocking of part of the Co surface. The Steady State Isotopic Thermal Kinetic Analysis (SSITKA) results on coverages and residence times were used to model the trend in TOF and methane selectivity as obtained under FT conditions. It was concluded that the lower TOF found for small cobalt particles (<6 nm) compared to larger ones is the result of a significant increase in the $CH_x$ residence time combined with a decrease of the $CH_x$ coverage. The higher methane selectivity of small Co particles obtained with FT conditions was mainly rationalized from the higher coverage of $H_2$.

## 2.4. Crystallographic properties of metallic cobalt

Cobalt can exist as two different allotropic phases: Face Centered Cubic (*fcc*) and Hexagonal Close Packed (*hcp*) with different catalytic properties.[59] The *fcc* and *hcp* cobalt phases are both closed packed structures in which each Co atom has twelve nearest neighbors. The difference between the phases is the stacking sequence of atomic planes in the (111) direction. The mode of activation, addition of promoters and different supports may influence the relative amounts of the phases formed during reduction. When a standard reduction procedure with a flow of $H_2$ at 350˚C is performed, mainly *fcc* cobalt is obtained.[48] The amount of *hcp* cobalt can be increased by a carbidization

procedure after reduction, during which the catalyst is treated with CO, turning *fcc* cobalt into $Co_2C$. Thereafter the carbidized cobalt is decarbidized with an $H_2$ treatment forming large amounts of *hcp* cobalt.[59,61] During catalytic tests performed by Ducreux et al. with alumina supported cobalt catalyst after a carbidization procedure, a 50% higher CO conversion was reported compared to a normally reduced catalyst having mainly *fcc* cobalt. *Hcp* $Co^0$ has a higher catalytic activity in FTS than *fcc* $Co^0$, caused by a higher amount of edges and kinks on the surface.[60] There was no significant difference in carbon selectivity reported between the two samples. Furthermore also the effect of noble metal promoters on the crystallographic phase of cobalt was studied. XRD analysis of a silica supported, ruthenium promoted cobalt catalyst showed a higher degree of *hcp* cobalt for the promoted catalyst compared to unpromoted catalyst and therefore had a higher activity during catalytic tests.[60]

## 2.5. Scope

During this research project the effect of noble metal promotion using different noble metals on Co FT catalysts in combination with a reducible support will be studied. The effect of activity, selectivity and stability of the noble metals Pt, Ru, Ag, Re will be studied. In literature an increased activity (turnover-frequency) for Pt and Ru promotion has been reported.[42,43] During this project the increased activity for the previously named noble metals will be studied in more detail. To study the properties of different noble metals various characterization techniques will be used: temperature programmed reduction (TPR), $H_2$-chemisorption, transmission electron microscopy (TEM), X-ray diffraction (XRD), In-situ X-ray diffraction and catalytic testing. By using TPR the reduction temperature and the degree of reduction is obtained. By $H_2$-chemisorption the metallic surface area is obtained, by which the dispersion can be determined. Futhermore the dispersion is also studied by TEM and XRD; TEM will also be used to study the dispersion of the spend catalysts. The measured dispersion of the cobalt particles is used in combination with catalytic testing at industrial conditions for the determination of the intrinsic activity of the catalysts. Besides that, the CO conversion and the CO conversion per gram of cobalt per second (CTY) and the selectivity's to the different carbon chains will be determined.

The scientific question of this project is: Does noble metal promotion, in different ratios, for cobalt Fischer-Tropsch catalysts on reducible oxides lead to an increase of the TOF? During this project will be tried to answer this question and hopefully also give a fundamental reason for the different activity and selectivities of the catalysts.

# 3. Synthesis and characterization of noble metal promoted $Co/TiO_2$

## 3.1. Theory of synthesis

Titania supported cobalt nanoparticles as catalyst for the FT reaction can be synthesized by using different methods: deposition precipitation, colloidal synthesis and incipient wetness impregnation. During this project incipient wetness impregnation is used as an easy and effective method for catalyst synthesis. Deposition precipitation and colloidal synthesis are not used in this project and are therefore not further discussed.[27,62]

The titania support is sieved before synthesis to ensure a constant grain size of the titania particles. This is crucial to ensure a constant flow of reactants and products through the reactor. If the grain size of the catalyst is too small, the catalyst clogs up the reactor and causes pressure drops over the reactor. Furthermore the pores of the titania crystallites should have the right size to prevent diffusion limitation of the reactants. In a diffusion-limited reaction, the rate of transport of the reactants through the reaction medium is the rate determining step, lowering the overall rate of reaction.[27]

Incipient wetness impregnation (IWI) is a simple and commonly used method for making cobalt FT catalysts. During IWI the support is impregnated with a solution of metal precursors, such as: cobalt(II)nitrate or cobalt(II)acetate. During this project water is used as solvent. Nitrates are popular precursors because of high solubility, good availability and cost effectiveness. High solubility ensures high loadings for single step impregnations. Acetates as precursor are used for catalysts with an highly disperse cobalt distribution, however carbon species (coke) may inhibit catalyst activity.[62,63]

In order to synthesize promoted cobalt FT catalysts via IWI, two different techniques can be used: co-impregnation and sequential impregnation. The impregnation of a support with a solution of multiple metal precursors (e.g. cobalt and a noble metal) is called co-impregnation. Co-impregnation is a simple method for synthesizing reproducible (noble) metal promoted cobalt catalyst of a certain cobalt/noble metal ratio. Furthermore, by complete mixing of the solution a homogeneous distribution of the precursor is ensured. Sequential impregnation involves multiple consecutive impregnation and drying steps with different precursor solutions containing one metal. This method is easier when multiple catalysts need to be synthesized with different promoter loadings, because only two precursor solutions are needed. However, a homogeneous distribution of the promoter and therefore the formation of bimetallic particles is not ensured.[62–64]

IWI can be performed in a vacuum to prevent adsorption of water and other molecules from the air during impregnation. Another possibility is to perform the impregnation in air directly after the drying procedure minimizing the adsorption from water and air molecules. During IWI the solution is added dropwise while stirring. The solution is drawn in the pores by capillary suction. It's essential for IWI to ensure proper wetting of the support without excess of solution outside the pores. Incipient wetness occurs when all pores of the support are filled with the liquid and there is no moisture outside the pores.[62]

The initial repartition of cobalt on the support depends to a larger extent on the type and concentration of hydroxyl groups on the surface and pH of impregnation solution. 4.00 M solutions of $Co(NO_3)_2 \cdot 6H_2O$ used during this project have a pH of ~5. The distribution of $Co^{2+}$ ions on the support after impregnation is affected by electrostatic interactions. Porous oxides such as alumina, silica, and titania have different points of zero charge (PZC). At a pH below the PZC, the surfaces of the

corresponding oxides are charged positively; at pH higher than the PZC, the surface of the support is charged negatively. If the impregnating solution has a pH below the PZC charge, repulsion between the surface of the support and $Co^{2+}$ atoms results in nonhomogeneous repartition of cobalt ions. At pH higher than the PZC, $Co^{2+}$ cations are distributed much more homogenously. Further increase in pH could lead to dissolution of the support in the impregnating solution. Titania P25 has a PZC of 6.3 which means that the surface of titania is neutrally charged at that pH.[65] At the stage immediately after impregnation, the interaction between the metal precursor and the support is relatively weak, thereby allowing redistribution of the active phase over the support body during drying and calcination.[51] After IWI a drying and heat treatment procedure is applied to evaporate the solvent, thereby increasing the concentration of the precursor to saturation and eventually crystallization. The hydrated salt particles (nitrates) melt at moderate temperatures (±200°C), which may cause the coalescence of their initially dispersed particles, or even their exclusion from the pores. After this treatment the majority of the cobalt particles on the surface will be in the fully oxidized state: $Co_3O_4$.

In literature has been reported that a heat treatment with small amounts of NO in the flow gas instead of $N_2$ ensures better particle distribution.

### 3.2. Experimental methods of the synthesis of noble metal promoted Co/$TiO_2$ catalyst

Titania P25 synthesized by Evonik GmbH is used as support and is a micro porous crystalline powder with a surface area of 50 $m^2/g$ and a pore volume of 0.3 ml/g. The pores of titania P25 are relatively large ensuring good reactant and product diffusion properties during FTS. In order to be suitable for use as a catalyst support in a laboratory scale FTS set-up, the support is sieved to a diameter between 75-150 µm. For each catalyst approximately 1.0 gram of support was used, which is sufficient for a catalytic run and further characterization. Before impregnation, the support is dried under vacuum and heated to ±100˚C in a round bottom flask for an hour.

The precursor solutions are prepared in volumetric flasks of 50 mL or 10 mL. The precursors in solid or liquid phase are weighed on a balance to obtain a 4.00 M solution of $Co(NO_3)_2 \cdot 6H_2O$ and a specific amount of noble metal. The density of the solution is accurately determined using a balance to weigh the solution. The density is used afterwards to determine the weight loading.

**Table 2**

| Precursor | Manufacturer | Purity (%) | Color code |
|---|---|---|---|
| $Co(NO_3)_2 \cdot 6H_2O$ (s) | Sigma-Aldrich | 99.99 | Black |
| $AgNO_3$ (s) | Sigma-Aldrich | 99 | Red |
| $Ru(NO)(NO_3)_3$ (s) | AlfaAesar | 98.2 | Blue |
| $[(NH_3)_4Pt](NO_3)_2$ (s) | Sigma-Aldrich | 99.995 | Green |
| $HReO_4$ (aq) | Sigma-Aldrich | 99.99 | Orange |

The solutions are prepared with different promoter concentrations and therefore catalysts with different noble metal loadings are obtained. The amount of promoter relative to the cobalt concentration is varied. In table the proposed mole ratios are displayed.

**Table 3**

| Noble metal/Co (at.) | wt. % noble metal |
|---|---|
| 0.0036 | 0.05-0.11 |
| 0.0071 | 0.10-0.21 |

| | |
|---|---|
| 0.0143 | 0.18-0.39 |

The deposition of the active metal occurs by co-impregnation via IWI in a 100 mL round bottom flask. A 4.00 M $Co(NO_3)_2 \cdot 6H_2O$ solution has a pH of ~5 which means that the surface of the titania is neutral. The solution is added drop wise using a syringe with a needle. The support is stirred using a magnetic stirrer during the impregnation. When 1.0 gram of titania P25 is impregnated to incipient wetness with a 4.00 M $Co(NO_3)_2 \cdot 6H_2O$ solution, the loading of the catalyst will be about 10 wt.% Co.

The weight loading was calculated by the equation:

$$\frac{m(Co)}{m(Co)+m(TiO_2)} * 100\% = \text{wt.\% Co} \quad (6)$$

$$\frac{m(\text{noble metal})}{m(\text{noble metal})+m(Co)+m(TiO_2)} * 100\% = \text{wt.\% noble metal} \quad (7)$$

After impregnation the samples are dried at 80°C for 2 hours in a fluidized bed of nitrogen with a flow of 350 ml/min. Thereafter the samples are heat treated in the same reactor at 250°C for 2 h with a fluidized bed of $N_2$ (350 ml/min) or in a fluidized bed of $N_2$, Ar and NO (350 ml/min of $N_2$ + 40 ml/min of 5% NO in Ar).

The standard drying procedure used during this project to obtain catalyst with a high dispersion was drying in a fluidized bed of $N_2$ at 80˚C for 2 hours followed by a heat treatment in a fluidized bed of $N_2$ at 250˚C for 2 hours.

Different drying procedures were applied to synthesize unpromoted catalysts with different dispersions to get a good image of the activity of the unpromoted catalysts with varying dispersion.

| **Drying and Heat treatment** | **Code** |
|---|---|
| Drying in a fluidized bed of $N_2$ at 80˚C for 2 hours<br>Heat treatment in a fluidized bed of **NO** at 250˚C for 2 hours | $N_2$(80)/NO(250) |
| Drying in static air at 60˚C for 24 hours<br>Heat treatment in a fluidized bed of $N_2$ at 250˚C for 2 hours | SA(60)/$N_2$(250) |
| Drying in static air at 60˚C for 24 hours<br>Heat treatment in a fluidized bed of **NO** at 250˚C for 2 hours | SA(60)/NO(250) |
| Drying in static air at 120˚C for 24 hours<br>Heat treatment in a fluidized bed of $N_2$ at 250˚C for 2 hours | SA(120)/$N_2$(250) |

Each catalyst is given a sample code to identify a certain catalyst. If the standard drying method is used, the drying method is not displayed in the sample code.

**Co** [weight loading of Cobalt in %] **noble metal** [weight loading of the noble metal in %] [the drying method]

Each specific sample is has a specific color code, as can been seen from table …

## 3.3. Experimental methods of catalyst characterization

### 3.3.1. Transmission electron microscopy

Transmission electron microscopy (TEM) measurements are performed on a FEI Tecnai 12 or a FEI Tecnai 20F with beam voltages of 120 kV and 200 kV respectively. The sample is prepared by immersing a small amount of catalyst in a test tube with ethanol. The test tube is put in an ultrasonic bath for a few seconds to make sure the catalyst particles are properly immersed in the solution. Then a Finn-pipette is used to immerse 0.3 µL of the solution onto a copper grid. Copper grids have a carbon film in which the catalyst particles can be deposited. The i-TEM software from AnalySIS, is used for particle size analysis of the TEM images.

Given below are the formulas used to determine the cobalt particle size. It was assumed that spend catalysts have particles with a metallic with a 2 nm shell of CoO. Formula 8 was used for fresh catalysts; formula 9 was used for spent catalysts and formula 10 was used to calculate the cobalt surface area.

$$d_{Co} = d_{Co_3O_4} \cdot 0.75 \quad (8)$$

$$d_{Co} = d_{CoO/Co} - \left(4 - \left(4 \cdot \frac{\rho_{CoO}}{\rho_{Co}}\right)\right) = d_{CoO/Co} - 1.11 \quad (9)$$

$$A_{Co} = \frac{6000}{\rho_{Co} \cdot d_{Co}} \quad (10)$$

$d_{Co}$ is the cobalt particle size in nm, $d_{Co3O4}$ is the cobalt(II,III)oxide particle size in nm, $d_{CoO/Co}$ is the spent cobalt particle size in nm, $\rho_{CoO}$ is the cobalt(II)oxide density 6,44 g/cm$^3$, $\rho_{Co}$ is the cobalt density: 8,90 g/cm$^3$, $A_{Co}$ is the cobalt surface area in m$^2$/g.

### 3.3.2. $H_2$ chemisorption

$H_2$ chemisorption is performed on a Micromeritics ASAP2020. ±200 mg of sample with a sieve fraction of 75-150 µm is used. At the start of each measurement the sample is reduced under a $H_2$ flow with a temperature ramp of 1˚C/min to 350˚C and then the temperature stays at 350˚C for 2 hours. Then a vacuum is applied on the tube to evacuate hydrogen and water. Thereafter the sample is cooled down to 140˚C and hydrogen is added in pulses to the sample. The measurement is performed at 140°C to ensure that hydrogen will be adsorbed at a high rate. The eventually obtained dispersion is used to calculate the cobalt surface area with formula 10.

### 3.3.3. X-ray diffraction

X-ray diffraction (XRD) measurements were performed on a Bruker D2 Phaser with a Cu Kα (λ=1.789 Å) X-ray source. ±300 mg sample with a sieve fraction of <75 µm was used for each measurement. The range of angles used was: 33-40° 2θ with a step size of 0.1° 2θ and a total measurement time of 30-50 sec/step. The average $Co_3O_4$ crystallite size was estimated by analysis of the 37° 2θ diffraction peak with an automatic calculation routine in DiffracEvaluation V2.0 software by Bruker, which is based on the Debye-Scherrer equation.

Debye-Scherrer equation:

$$\tau = \frac{K\lambda}{\beta \cos\theta} \quad (11)$$

K is a dimensionless shape factor. The shape factor has a typical value of about 0.93, but varies with the actual shape of the crystallite; λ is the X-ray wavelength (λ=1.789 Å); β is the line broadening at half the maximum intensity (FWHM), after subtracting the instrumental line broadening displayed in radians; θ is the Bragg angle of the analyzed peak. $\tau$ is the mean size of the crystalline domains, which may be smaller or equal to the grain size since grains consist of one or more crystalline domains. By using equation 8 the eventual cobalt particle size is obtained.

### 3.3.4. In-situ X-ray diffraction

In-situ XRD measurements were performed using a Bruker AXS D8 Advanced equipped with a Siemens KFL-Cu-2K light source (λ=1.541 Å). A small amount (~50 mg) of catalyst (>75 μm) was placed in an in-situ cell with temperature and gas feed control. The range of angles used was 33˚-65˚ 2θ with a step size of 0.05˚ 2θ. The sample was placed in a The catalyst was reduced under a flow of $H_2$(25%)/He(75%) and a temperature ramp of 1˚C/min starting at 50˚C to 350˚C. Meanwhile between every 20 minutes (Δ20˚C) diffraction patterns were measured.

### 3.3.5. Temperature programmed reduction

Temperature programmed reduction (TPR) measurements were performed using a Micromeritics ASAP 2920. The first step was the drying of the sample by heating to 500°C after which the sample was cooled to ambient conditions. Then the sample was gradually reduced under a flow of 5% $H_2$/Ar (50 mL/min) while heating to 500°C with a ramp of 5°C/min. The hydrogen consumption during reduction was measured with a TCD detector.

### 3.4. Results of catalyst synthesis

The results from XRD and TEM experiments reveal that ~10 wt.% $Co/TiO_2$ FT catalysts where synthesized successfully. As can be seen in figure 9 small $Co_3O_4$ diffraction peaks are visible in the XRD diffraction pattern. Also diffraction patterns of noble metal promoted catalyst were measured, but no noble metal oxide species were observed in the diffraction pattern, since the molar amount of noble metals is too low.

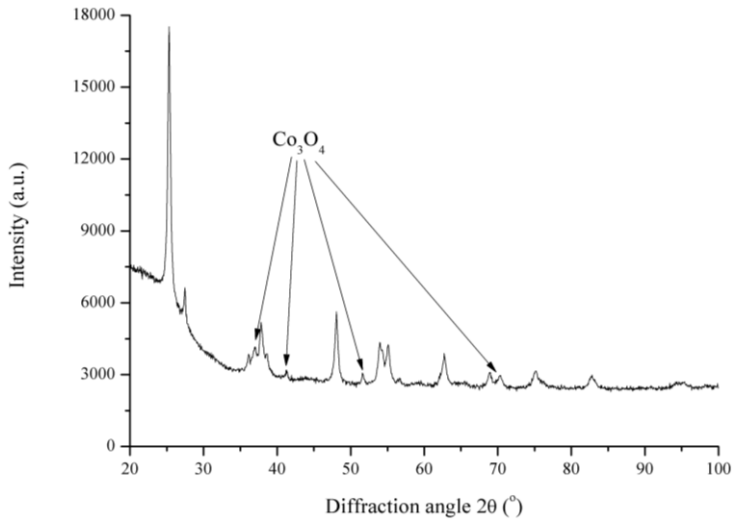


**Figure 9: Diffraction pattern of a $Co/TiO_2$ catalyst after heat treatment. The diffraction peaks of $Co_3O_4$ are indicated.**

From TEM analysis can be seen that $Co_3O_4$ particles are present on the surface of the support.

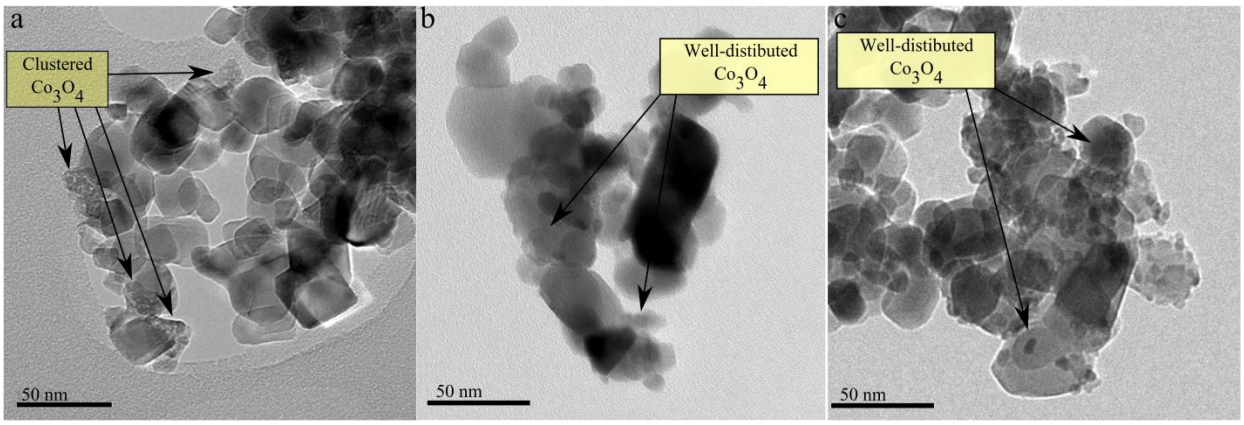


**Figure 10** a: **Co9,46-SA120/$N_2$** b: **Co9,41-$N_2$** c: **Co9,61-$N_2$/NO.**

NOBLE METAL PROMOTED

### 3.5. Results of cobalt particle size studies

The average cobalt particle size was determined for each catalyst with three different characterization methods: XRD, $H_2$ chemisorption and TEM. The results of XRD and TEM were in good agreement with each other as can be seen in figure 11. The cobalt particle sizes for the catalyst dried in a fluidized bed vary between 4 and 6 nm. The catalysts dried in static air have a larger average cobalt particle size. For fresh catalyst no clear dependence of the presence of noble metals on the cobalt particle size was seen.

For TEM imaging approximately 200 particles per sample where measured, mainly depending on the amount of particles that could be distinguished on the images. The standard deviation of the TEM measurements varied between 1.62 and 3.19 nm which can be explained by polydispersity of the cobalt particles, or by inaccuracies in the measurement. Due to the low contrast differences between cobalt oxide and titania particles, distinguishing the different species on TEM images can be difficult. From XRD measurements the average size of $Co_3O_4$ crystallite domains is obtained, which might differ from the true $Co_3O_4$ particle size because particles can consist of multiple crystallite domains or inhibit crystallographic defects. Furthermore the sensitivity of the XRD device used, was limited for measuring for 10 wt.% $Co/TiO_2$.

From the particle size study by can be concluded that the fresh unpromoted and promoted catalysts synthesized with the standard drying method have very similar dispersions. Both the TEM and the XRD results show a very good conformity towards an average cobalt particle size of ~6 nm. This is in accordance with earlier TEM and $H_2$ chemisorption studies reporting 7-9 nm cobalt particles for IWI and drying in a fluidized bed.[48,63,66]

From the results can be seen that different synthesis techniques for the unpromoted $Co/TiO_2$ result in catalysts with different dispersions. Co9,46-SA(120)/$N_2$(250) has clearly a larger average particle size compared to the other catalysts caused by a different drying method. Multiple articles report larger cobalt particle sizes for catalysts dried in static air.[33,67]

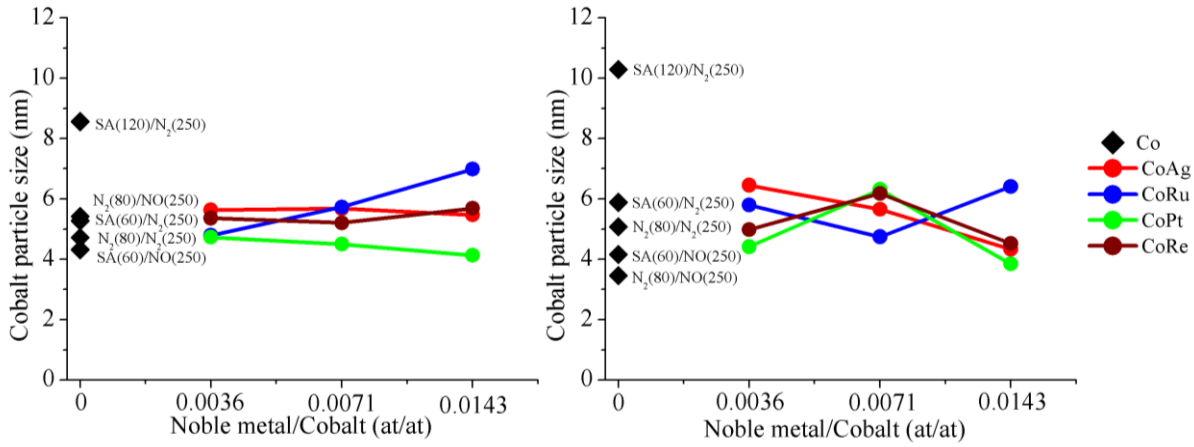


**Figure 11: Results of TEM particle size analysis of fresh $Co/TiO_2$ (left) and of XRD $Co/TiO_2$ (right) catalysts.**

The results from $H_2$ chemisorption experiments yielded the cobalt surface area which could be converted to the cobalt particle size. As can be seen in figure 12, the results are not coherent with the results from XRD and TEM experiments. The cobalt particle sizes of the promoted samples are between 15-30 nm whereas the cobalt particle sizes for the unpromoted samples are even higher; between 27-40 nm.

Similar cobalt particle sizes were obtained by $H_2$ chemisorption for noble metal promoted and unpromoted $Co/TiO_2$ in multiple articles.[43,49,63,68] The results of these articles can sometimes be explained by different synthesis methods such as IWI in combination with drying at elevated temperatures (80-120°C) in static air, yielding catalyst with a high average cobalt particle size. An article by Oukaci et al. cobalt particle sizes for IWI prepared, unpromoted $Co/TiO_2$ of 40 nm and 38 nm were reported for $H_2$ chemisorption and XRD, respectively. In the same article ruthenium promoted $Co/TiO_2$ had a $H_2$ chemisorption particle size of 19 nm and an XRD particle size of 39 nm.[49] However, these results cannot explain the difference in results between $H_2$ chemisorption and XRD and TEM. Other studies however reported $H_2$ chemisorption values corrected for the degree of reduction of the cobalt.[48,66] A study by Holmen et al. reports the presence of partly reduced cobalt (degree of reduction of 69%, determined by $O_2$-titration) on unpromoted $Co/TiO_2$ after reduction at 350°C under a flow of $H_2$. Meanwhile a rhenium promoted $Co/TiO_2$ had a degree of reduction of 71%. In studies by Li et al. using similar techniques unpromoted $Co/TiO_2$ had a degree of reduction of 52% after reduction. Therefore the apparent particle size obtained by $H_2$ chemisorption of 20 nm was corrected to 11 nm. Furthermore, a ruthenium promoted $Co/TiO_2$ with a degree of reduction of 64% with an apparent particle size of 13 nm was corrected to 8.5 nm and for rhenium promoted $Co/TiO_2$ a similar result was obtained; a degree of reduction of 61% leading to a correction of 13 nm to 8.1 nm. The corrected values are in reasonable agreement with the results of TEM and XRD. Unfortunately, the integration of the TCD signal of the TPR experiments yielded doubtful results; therefore we could not perform a good correction on our $H_2$ chemisorption results. Another explanation can be SMSI effects during the reduction of $Co/TiO_2$, causing mixed oxide patches migrating over the surface onto cobalt particles. This reduces the cobalt metal surface and therefore increases the apparent particle size.[20,68]

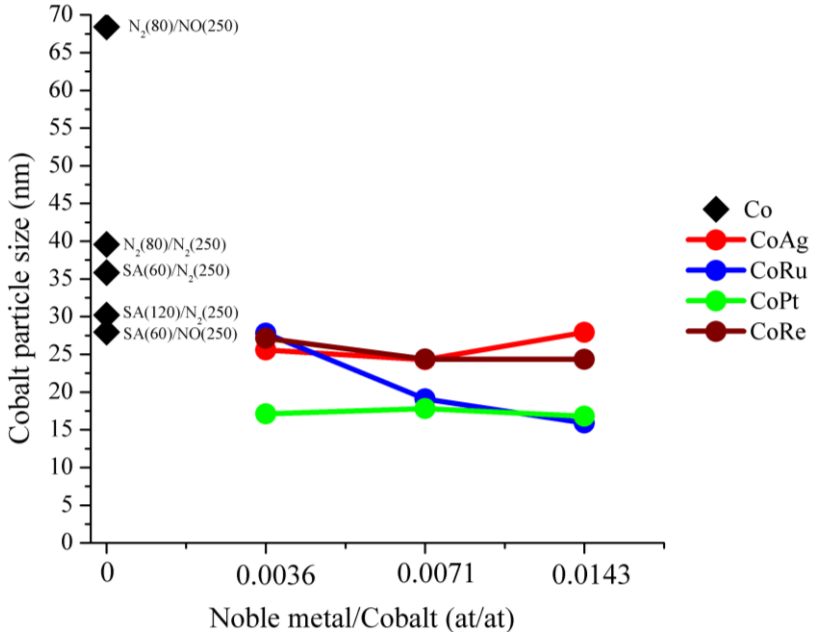


**Figure 12: Results of particle size study with $H_2$ chemisorption.**

## 3.6. Results of temperature programmed reduction experiments

The reduction temperatures noble metal promoted $Co/TiO_2$ catalysts were studied with TPR as can be seen in figure 13. The TCD detector signal is plotted on the y-axis while the temperature is plotted on the x-axis. The first peak in the TPR profile is caused by the reduction of $Co_3O_4$ to CoO, the second peak is caused by the reduction of CoO to Co.[31]

The peaks of the TPR profiles tend to shift to lower temperatures with increasing noble metal promoter ratio caused by the hydrogen spillover effect. Another explanation for reduction at lower temperatures is the formation of bimetallic particles. For the sliver promoted catalyst a slight shift is seen in the reduction peaks with increasing silver loading. A similar result was obtained by T. Jermwongratanachai et al. for an alumina supported cobalt FT catalyst: the addition of silver facilitated the reduction of cobalt oxides.[69] For platinum a large shift is seen for all platinum loadings; there is no difference between platinum promoted samples. In literature has been reported that already small amounts (<0,1 wt.%) of platinum can facilitate the reduction of cobalt oxide significantly. This is caused by the excellent hydrogen splitting capability of platinum thereby acting as a catalyst for cobalt oxides reduction.[31] For ruthenium an increasing shift is seen for increasing ruthenium loading is observed. The effect is more pronounced than for the silver promoted catalyst which is in accordance with literature results obtained on alumina.[69] The rhenium promoted samples show a clear shift in the second peak while the first peak shows only a slight shift. In literature this has been explained by the reduction of rhenium oxide at nearly the same temperature as the first reduction step ($Co_3O_4 \rightarrow CoO$) of cobalt oxides. Therefore the distortions in the signal below 150°C are most likely caused by the decomposition of nitrates of the cobalt precursor.

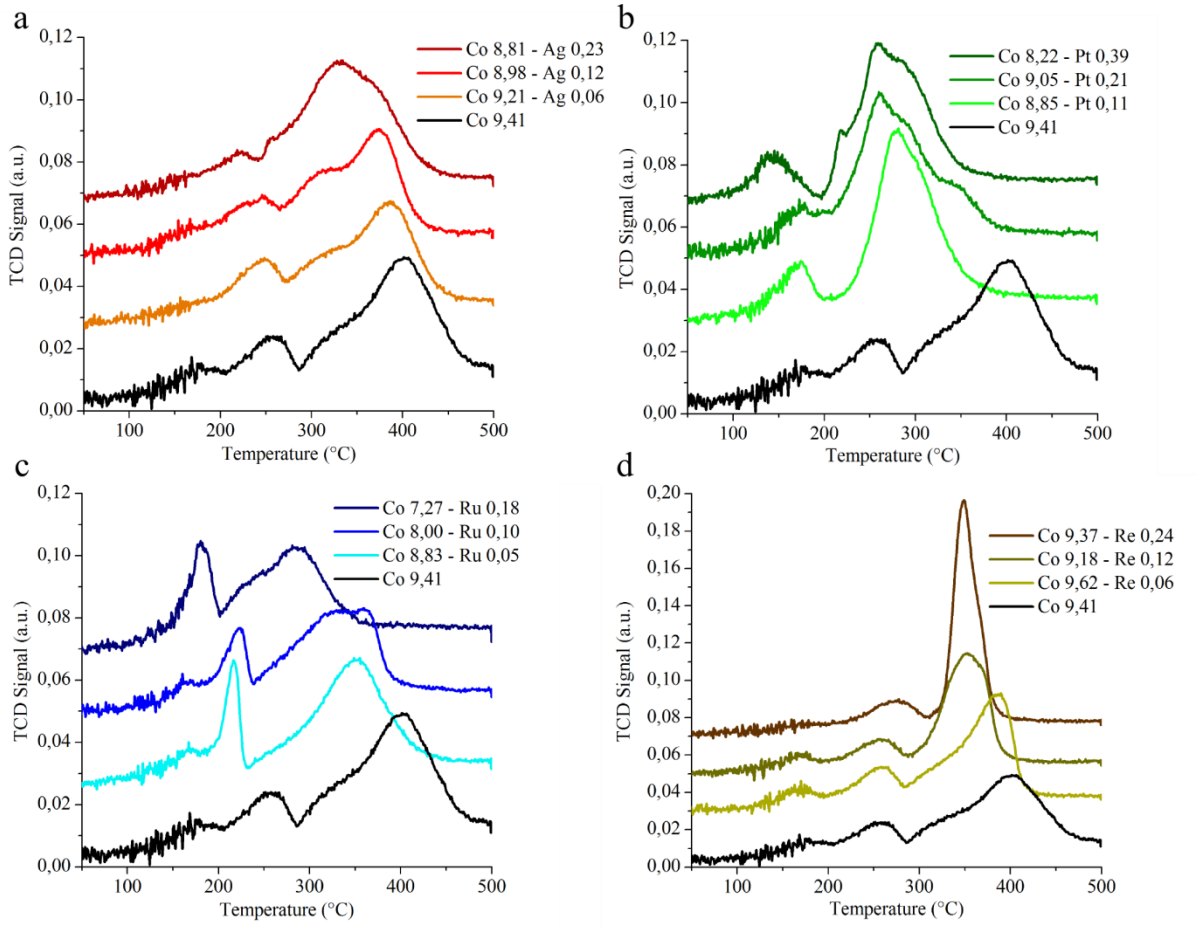


**Figure 13: TPR profiles of a: silver promoted b: platinum promoted c: ruthenium promoted d: rhenium promoted $Co/TiO_2$ catalysts compared with an unpromoted sample.**

### 3.7. Results of in-situ x-ray diffraction experiments

From the diffraction patterns in figure 14 the unpromoted and silver promoted samples can be seen. It can be concluded that the reduction of cobalt occurs from $Co_3O_4$ to CoO to metallic cobalt. The black, blue and grey patterns are from the unpromoted catalyst whereas the orange, red and purple patterns are from the silver promoted catalyst. The black and orange patterns were in both cases taken at room temperature before the reduction treatment. The peaks from $Co_3O_4$ and CoO can be distinguished indicating the presence of both species on fresh catalysts. The blue and red patterns are taken at ±235°C where an increased amount of CoO can be seen at 49° 2θ compared to the pattern taken at room temperature. This can be confirmed by the TPR patterns from figure 13 indicating the reduction of $Co_3O_4$ starting at ±235°C. Furthermore a small peak at 52° 2θ appears, probably caused by the presence of metallic cobalt. In the pattern taken at 360°C the CoO peak disappears, however a peak at 52° 2θ appears caused by metallic cobalt. The peaks caused by metallic cobalt of both *fcc* and *hcp* are very near to each other which makes interpretation difficult. Furthermore, because the catalysts used have a low cobalt weight loading and the diffraction detector has a low sensitivity, the quantification of the metallic cobalt of the different phases is hard. Nevertheless, in the silver promoted sample a shoulder on the right side of the metallic cobalt peak can be seen absent in the pattern of the unpromoted catalyst. This shoulder could indicate an increased amount of cobalt *hcp* in the silver promoted sample compared to the unpromoted sample leading to a higher catalytic activity.

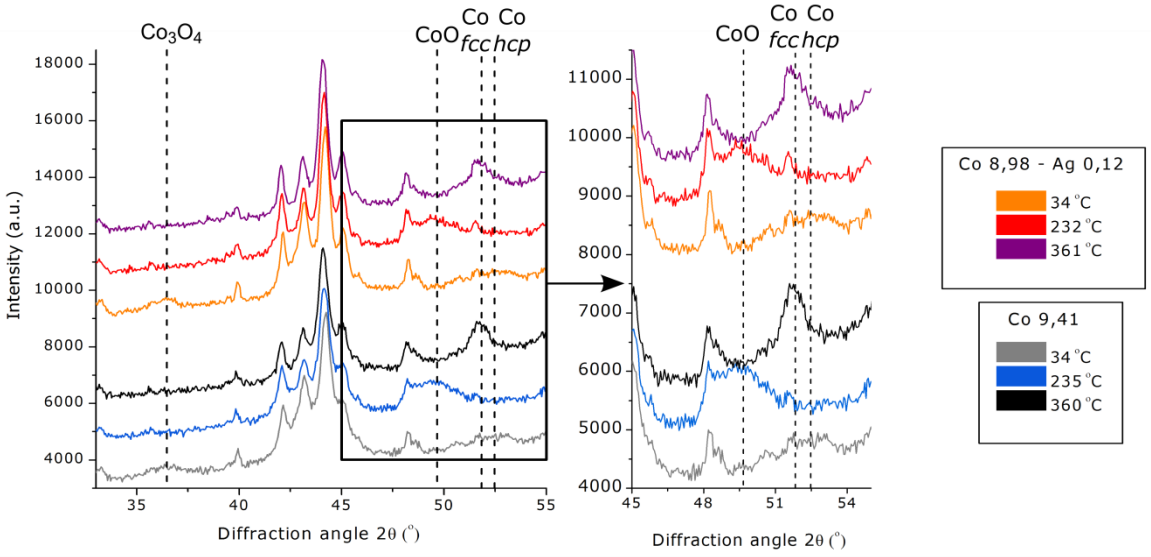


**Figure 14: In-situ XRD of Co/TiO2 and silver promoted Co/TiO2**

### 3.8 conclusions of characterization results

Based on the TEM and XRD results can be concluded that 10 wt.% $Co/TiO_2$ catalysts were successfully synthesized. $Co_3O_4$ particles were observed on the surface of $TiO_2$ and $Co_3O_4$ peaks were observed in the diffraction pattern.

The TPR performed on different catalysts with different promoter ratio yielded interesting results. The biggest improvements were seen for the platinum and ruthenium promoted samples. These noble metals significantly decreased the reduction temperature. Rhenium and silver were less effective in facilitating the reduction of cobalt oxide.

From the in-situ XRD measurements can be seen that metallic cobalt is formed after a reduction procedure. From the diffraction patterns some evidence of a increased amount *hcp* cobalt for the silver promoted catalyst compared to the unpromoted catalyst can be seen.

# 4. Catalytic performance of noble metal promoted $Co/TiO_2$ Fischer-Tropsch catalysts

## 4.1. Introduction

The catalytic performance of $Co/TiO_2$ FT catalysts are tested in a catalytic testing set-up (Avantium Florence W16). The set-up has 16 parallel fixed bed reactors which can operate under high pressure, which makes the set-up suitable for high alpha FTS (HP, LTFT). At high pressures (20 bar) the FTS has a higher selectivity for $C_{5+}$ products compared to FTS at atmospheric pressure. The reaction products were analyzed using online gas chromatography (GC) (Agilent 7890A).

## 4.2. Experimental methods

The reactors used for the catalytic testing set-up are from stainless steel with an inner diameter of 2 mm and a length of 15,5 cm. The reactors are loaded with a homogeneous mixture of 50 mg $Co/TiO_2$ catalyst with a sieve fraction of 75-150 µm and 100 µl SiC (sieve fraction: ~200 µm) as diluent. For the unpromoted catalyst 70 mg of $Co/TiO_2$ was used to ensure equal CO conversions under the same conditions. The flow of gas through the reactor enters from the top of the reactors and the product stream leaves from the bottom.

In advance of the catalytic test the samples are dried in a He steam for 2 h. Then the catalyst is activated by reduction of cobalt oxide in a $H_2$/He (1/3) flow at 350˚C for 8 hours with a ramp of 1˚C/min. Subsequently, the reactors are cooled to 180˚C and pressurized to 20 bar under a flow of $H_2$. Then the flow is switched to $H_2$/CO (2/1) and the temperature was increased to 220˚C (1˚C/min). The standard gas hourly space velocity (GHSV) of the flow in the reactors was 2000 $h^{-1}$. During the measurement changes in the GHSV and temperature could be made.

The reaction products were analyzed using online GC with a thermal conductivity detector (TCD) and a flame ionization detector (FID) detector. All 16 reactors are connected to a selection switch going to the GC to analyse the product streams one by one. The permanent gases were separated on a Shincarbon column in combination with a TCD detector and quantified against He as an internal standard. The different carbon chains are separated on a PPQ column in combination with a FID detector and is quantified against the TCD signal of the internal standard He. The metallic surface area of cobalt obtained from $H_2$-chemisorption was entered in the software of the Flowrence to calculate the TOF of the different samples.

Formulas for calculating CO conversion ($X_{CO}$), Cobalt time yield (CTY), Turn over frequency (TOF) and $C_{5+}$ selectivity ($S_{C_{5+}}$) are displayed below. $f_{CO,in}$ is the flow of CO going in the reactor in Nml/min; $f_{H_2,in}$ is the flow of $H_2$ going in the reactor in Nml/min; $N_{C_n}$ is the amount of carbon atoms detected in the reaction products of length in mole; $m_{Co}$ is the mass of cobalt in the sample in g; $S_{Co}$ is the atomic surface area of cobalt in $m^2$. $A_{Co}$ is the metallic surface area of cobalt in $m^2$; $N_A$ is Avogadro's number: $6{,}02 \cdot 10^{23}$ $mol^{-1}$.

$$X_{CO} = \frac{f_{CO,in} - f_{CO,out}}{f_{CO,in}} \cdot 100\%$$

$$CTY = \frac{f_{CO,in} \cdot X_{CO}}{m_{Co}}$$

$$TOF = \frac{f_{CO,in} \cdot X_{CO} \cdot S_{Co}}{A_{Co} \cdot m_{Co} \cdot N_A} = CTY \cdot \frac{S_{Co}}{A_{Co} \cdot N_A}$$

$$S_{C_{5+}} = 1 - \frac{\sum_1^4 (N_{C_n} \cdot n)}{f_{CO,in} \cdot X_{CO}} \cdot 100\%$$

$$GHSV = \frac{\sum V_{gasflow}}{V_{cat} \cdot t_h}$$

## 4.3. Results of catalytic test

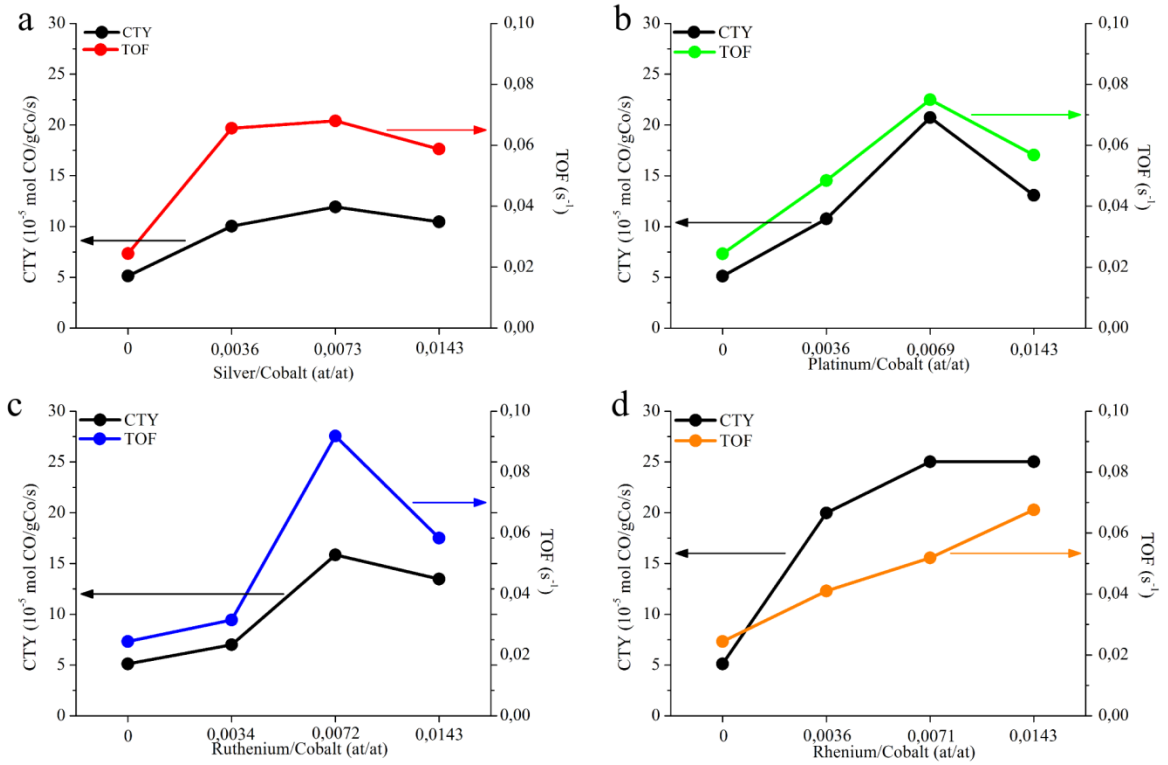


**Figure 15: Catalytic activity of unpromoted and noble metal promoted Co/$TiO_2$ FT catalyst. 20a: silver promoted; 20b: platinum promoted; 20c: ruthenium promoted; 20d: rhenium promoted. The cobalt time yield is plotted on the left y-axis while the turn over frequency is plotted on the right y-axis.**

In figure 20 the results of different samples of the catalytic test are displayed. The dispersion was determined with TEM after reduction and after catalysis. In figure 20a the results of the reaction with the silver promoted Co/$TiO_2$ catalyst are displayed.

A three-fold increase in TOF can be seen by promotion with silver with low and higher cobalt/silver ratios which is mainly caused by dispersion effects. As can be seen in table 5 the particle size of the silver promoted Co/$TiO_2$ catalyst increases significantly during reduction and catalytic testing compared to the fresh catalyst, lowering the amount of active sites. The CTY of the catalyst however stays the same thereby giving the catalyst a higher apparent intrinsic activity.

A three-fold increase in TOF can also be seen for the medium platinum promoted sample. There seems to be an optimum in promoter loading since the catalyst with a platinum/cobalt ratio of 0,0143 and 0,0036 have a lower activity than with a ratio of 0,0069.

A four-fold increase in TOF can be seen for the medium ruthenium promoted sample. This can be explained partly by an increased cobalt time yield and partly by an increased dispersion lowering the amount of active sites.

For rhenium promoted samples a two-fold increase in the TOF can be observed. This can be explained by an greatly increased CTY. A reason for this increasing CTY can be the low average particle size causing a large number of active sites.

**Table 4: Overview of the catalytic data of all samples. The unpromoted catalyst with a cobalt loading of 10,25 wt.% and the rhenium promoted samples were measured with a GHSV value of 4000h$^{-1}$; whereas the other catalyst were measured with a GHSV of 2000h$^{-1}$. The particle size was determined with TEM analysis after reduction and catalysis.**

| Catalyst | $d_p$ (nm) | $d_p$ (nm) | $X_{CO}$ (%) | CTY ($\cdot 10^{-5}$ mol CO/$g_{Co}$/s) | TOF fresh ($s^{-1}$) | TOF spent ($s^{-1}$) | $S_{C1}$ (%) | $S_{C2-C4}$ (%) | $S_{C5+}$ (%) | $C_3H_6$/ $C_3H_8$ |
|---|---|---|---|---|---|---|---|---|---|---|
| Co 9,41 | 5,27 | 8,60 | 21,96 | 5,13 | 0,015 | 0,024 | 7,1 | 7,4 | 85,4 | 3,3 |
| Co 9,46 | 8,56 | 5,06 | 29,97 | 7,10 | 0,034 | 0,020 | 6,3 | 5,9 | 87,8 | 3,0 |
| Co 9,20 | 4,32 | 5,85 | 30,86 | 7,53 | 0,018 | 0,024 | 6,3 | 5,6 | 88,1 | 2,3 |
| Co 10,25 | 4,72 | 3,23 | 28,20 | 12,27 | 0,032 | 0,022 | 5,3 | 3,5 | 91,2 | 2,9 |
| Co 9,61 | 5,42 | 5,20 | 26,53 | 6,13 | 0,018 | 0,018 | 6,2 | 5,5 | 88,3 | 3,2 |
| Co 9,21 Ag 0,06 | 5,63 | 11,80 | 30,30 | 10,04 | 0,031 | 0,066 | 6,5 | 5,0 | 88,6 | 2,8 |
| Co 8,98 Ag 0,12 | 5,68 | 10,29 | 33,93 | 11,93 | 0,038 | 0,068 | 6,4 | 5,0 | 88,6 | 2,4 |
| Co 9,9 Ag 0,26 | 5,79 | 10,14 | 33,08 | 10,47 | 0,034 | 0,059 | 7,0 | 6,0 | 87,0 | 2,2 |
| Co 8,83 Ru 0,05 | 5,47 | 8,11 | 20,08 | 7,01 | 0,021 | 0,031 | 7,3 | 8,1 | 84,6 | 4,0 |
| Co 8,00 Ru 0,10 | 5,73 | 10,46 | 40,91 | 15,85 | 0,050 | 0,092 | 5,9 | 4,6 | 89,5 | 2,7 |
| Co 7,27 Ru 0,18 | 6,99 | 7,82 | 31,78 | 13,47 | 0,052 | 0,058 | 7,0 | 5,2 | 87,8 | 3,0 |
| Co 8,85 Pt 0,11 | 4,73 | 8,13 | 30,44 | 10,75 | 0,028 | 0,048 | 7,6 | 9,5 | 82,9 | 3,1 |
| Co 9,05 Pt 0,21 | 4,50 | 6,53 | 59,81 | 20,74 | 0,052 | 0,075 | 5,7 | 4,9 | 89,4 | 1,9 |
| Co 8,22 Pt 0,39 | 4,13 | 7,85 | 34,17 | 13,08 | 0,030 | 0,057 | 7,3 | 9,3 | 83,4 | 2,9 |
| Co 9,58 Re 0,06 | 5,37 | 3,70 | 30,86 | 19,98 | 0,059 | 0,041 | 6,2 | 4,0 | 89,8 | 1,9 |
| Co 9,72 Re 0,13 | 5,21 | 3,74 | 38,99 | 25,02 | 0,072 | 0,052 | 5,7 | 3,8 | 90,5 | 2,0 |
| Co 9,76 Re 0,25 | 5,69 | 4,88 | 39,53 | 25,02 | 0,079 | 0,068 | 5,7 | 4,0 | 90,2 | 2,1 |

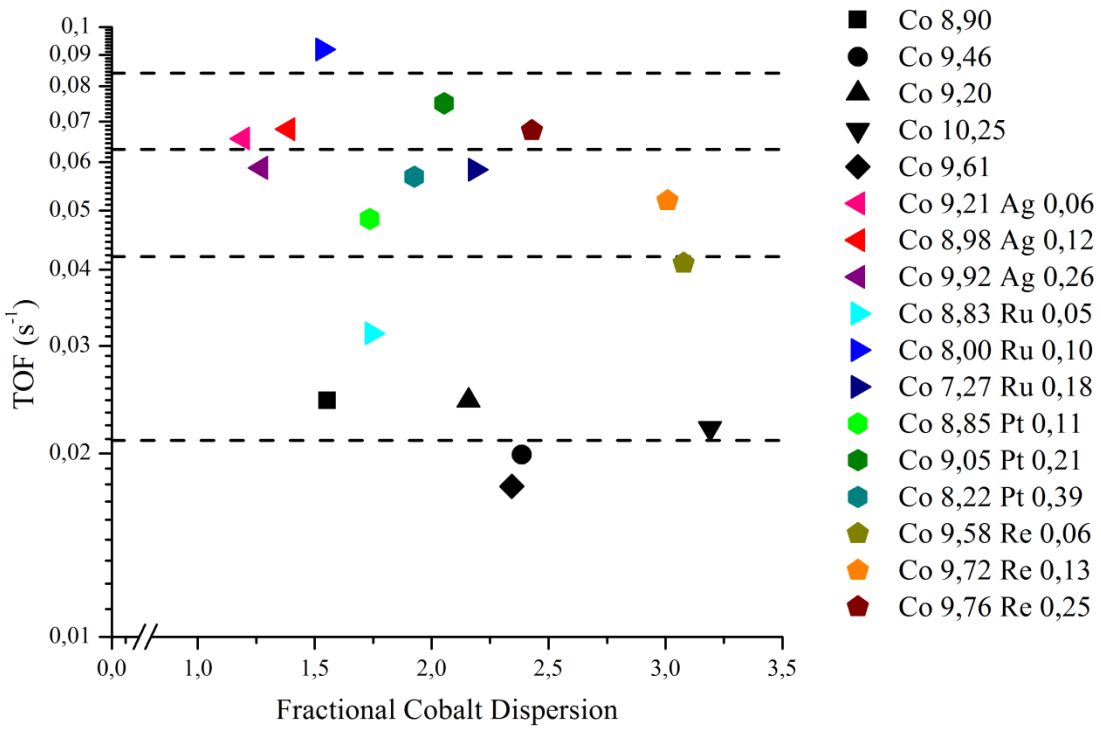


**Figure 16: Results of catalytic testing of all samples. The dotted lines are a guide to the eye and represent the multiplications in the TOF.**

The lowest dotted line represents the average TOF of the unpromoted samples, whereas the dotted lines above this line represent the multiplications of this average unpromoted TOF. It could be concluded that the silver promoted samples have a three-fold higher turnover frequency compared to the unpromoted samples regardless of the promoter loading. Furthermore, a four-fold increase in activity can be reported for a ruthenium sample with a medium promoter loading, whereas the ruthenium promoted samples with a low and a high promoter loading have lower activities. The platinum promoted catalyst also have an three times higher intrinsic activity with the medium promoted sample as the most active. The rhenium promoted catalyst have a 2-3 fold higher activity with the 'heavy' promoted sample as most active. In table 5 an overview is given of all the tested catalysts with a number of reaction parameters. It has been tried to keep the CO conversion during the tests in the range of 20-40 during the catalytic tests to suppress the negative effect of the water-gas shift reaction.

## 4.4 Comparison with literature TOF values

For a comparative study results of H2 chemisorption were used to allow literature comparison.

Unfortunately there is a large difference in TOF values for the unpromoted co/Tio2 used during our project.

The H2 chemisorption experiments did not yield very accurate results.

As can be seen in Figure 18, the activities of the promoted samples correspond well with literature values. Studies of Holmen and Iglesia were used. Holmen performed FTS at 210, Iglesia t 200. Results were adjusted using the Nernst equation. Furthermore, a review article by Bartholomew was used to obtain results

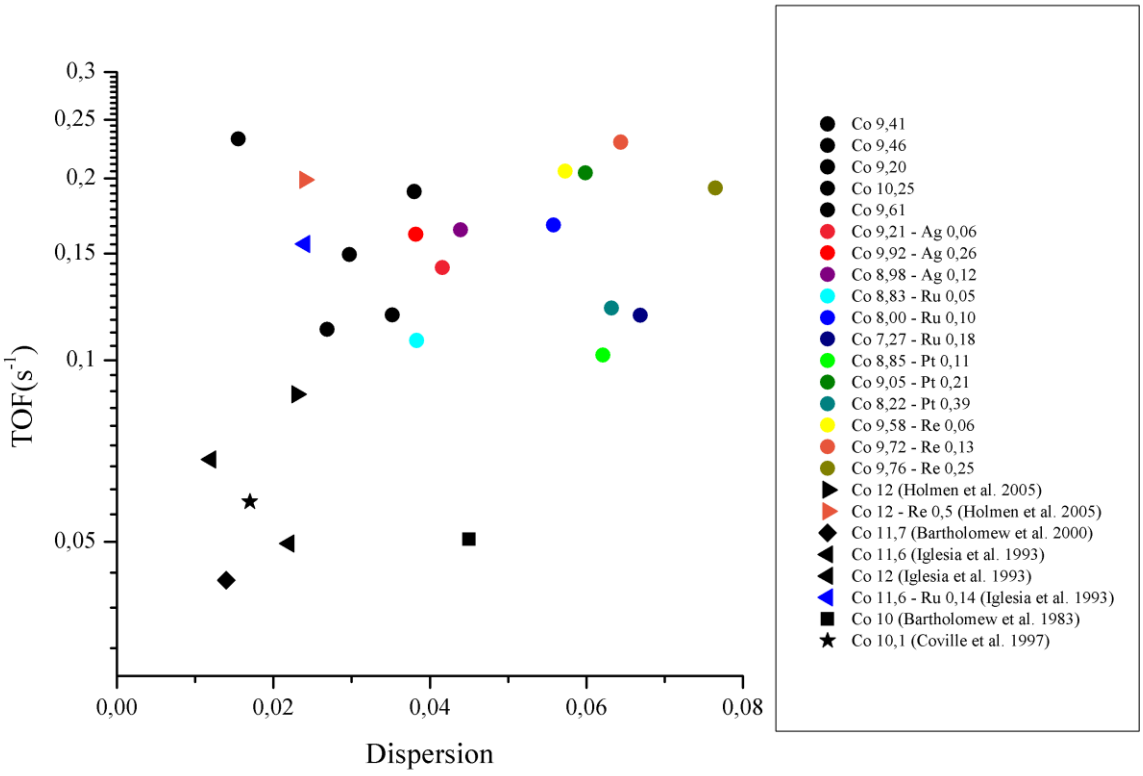


**Figure 17: Graph with TOF value's from literature.**

## 4.5. Discussion and conclusions

From the catalytic tests can be seen that by promotion with a noble a higher cobalt time yield and turnover frequency is obtained. The average TOF obtained for unpromoted catalyst with different dispersion was 0,0023 $s^{-1}$. For the silver and platinum promoted catalysts a threefold increase in TOF was observed. The TOF for the silver promoted catalyst was notdepended on the Co/Ag ratio. Howerever, the TOF for the platinum was dependend on the Co/Pt ratio. The highest activity was observed for the medium promoted catalyst. For the ruthenium promoted sample a four-fold increase was observed which depended highly on the promoter ratio. The highest TOF was observed for the medium ruthenium promoted catalyst. For the rhenium promoted catalyst a two fold increase was observed. The TOF increased with increasing rhenium ratio.

The $C_{5+}$ selectivities for the platinum promoted catalyst were significantly lower compared to the unpromoted catalysts. This can be explained by a selectivity towards short olefins for platinum itself. The $C_{5+}$ selectivities for the other catalysts are more or less the same.

The particle size study from the spent catalysts. The rhenium promoted samples show a smaller average particle size which could be attributed to the dispersion promoting effects.[20] The other promoted samples show a larger average particle size caused by coalescence of the cobalt particles during reduction and synthesis. Especially the silver and ruthenium promoted catalysts are prone to coalescence causing an significantly increased average particle size. The $H_2$ chemisorption measurements yielding the dispersion from the metallic surface area, show a different view of the dispersion.

# 5. Conclusions

During this project several noble metal promoted $Co/TiO_2$ catalyst were synthesized successfully. The catalysts have a cobalt weight loading between 7.3 – 10.2 wt. % and a noble metal /cobalt (at/at) ratio between 0.0034-0.0143at.

Based on the TEM and XRD results can be concluded that $Co/TiO_2$ catalysts were successfully synthesized. $Co_3O_4$ particles were observed on the surface of $TiO_2$ and $Co_3O_4$ peaks were observed in the diffraction pattern.

From the particle size study by can be concluded that the fresh unpromoted and promoted catalysts synthesized with the standard drying method have very similar dispersions. Both the TEM and the XRD results show a very good conformity towards an average particle size of ~6 nm. The catalyst that was dried at a 120 °C has a significant larger average particle size. The particle size study from the spent catalysts shows different results. The rhenium promoted samples show a smaller average particle size which could be attributed to the dispersion promoting effects.[20] The other promoted samples show a larger average particle size caused by coalescence of the cobalt particles during reduction and synthesis. Especially the silver and ruthenium promoted catalysts are prone to coalescence causing an significantly increased average particle size. The $H_2$ chemisorption measurements yielding the dispersion from the metallic surface area, show different results. Because the hydrogen adsorption was lower than expected from a higher average particle size was yielded

The TPR performed on different catalysts with different promoter ratio yielded interesting results. The biggest improvements were seen for the platinum and ruthenium promoted samples. These noble metals significantly decreased the reduction temperature. Rhenium and silver were less effective in facilitating the reduction of cobalt oxide.

From the in-situ XRD measurements can be seen that metallic cobalt is formed after a reduction procedure. From the diffraction patterns some evidence of an increased amount hcp cobalt for the silver promoted catalyst compared to the unpromoted catalyst can be seen.

From the catalytic tests can be seen that by promotion with a noble a higher cobalt time yield and turnover frequency is obtained. The average TOF obtained for unpromoted catalyst with different dispersion was 0,0023 $s^{-1}$. For the silver and platinum promoted catalysts a threefold increase in TOF was observed. The TOF for the silver promoted catalyst was notdepended on the Co/Ag ratio. Howerever, the TOF for the platinum was dependend on the Co/Pt ratio. The highest activity was observed for the medium promoted catalyst. For the ruthenium promoted sample a four-fold increase was observed which depended highly on the promoter ratio. The highest TOF was observed for the medium ruthenium promoted catalyst. For the rhenium promoted catalyst a two fold increase was observed. The TOF increased with increasing rhenium loading.

The $C_{5+}$ selectivities for the platinum promoted catalyst were significantly lower compared to the unpromoted catalysts. This can be explained by a selectivity towards short olefins for platinum itself. The $C_{5+}$ selectivities for the other catalysts are more or less the same.

# References


(1) Khodakov, A. Y.; Chu, W.; Fongarland, P. *Chem. Rev.* **2007**, *107*, 1692–1744.

(2) Sabatier, P.; Senderens, J. B. *Comptes Rendus l'Académie des Sci. Paris* **1902**, *134*, 689–691.

(3) Sabatier, P.; Senderens, J. B. *Comptes Rendus l'Académie des Sci. Paris* **1902**, *134*, 1902.

(4) Sabatier, P.; Senderens, J. B. *Comptes Rendus l'Académie des Sci. Paris* **1902**, *134*, 1185–1188.

(5) Mittasch, A.; Schneider, C. BASF, German Patent DRP 293, 1913.

(6) Mittasch, A.; Schneider, C. BASF, German Patent DRP 295, 1914.

(7) Mittasch, A.; Schneider, C. BASF, German Patent DRP 295, 1914.

(8) Mittasch, A.; Schneider, C. *United States Pat. Off.* **1916**, 3.

(9) Fischer, F.; Tropsch, H. *Brennstoff-Chemie* **1923**, *193*, 276.

(10) Fischer, F.; Tropsch, H. *Brennstoff-Chemie* **1924**, *5*, 201.

(11) Fischer, F.; Tropsch, H. *Brennstoff-Chemie* **1926**, *7*, 97.

(12) Fischer, F.; Koch, H. *Brennstoff-Chemie* **1932**, *13*, 61.

(13) History Max-Planck-Institut für Kohlenforschung http://www.kofo.mpg.de/en/institute/history.

(14) Antonides, L. E. *United States Geol. Surv.* **1997**.

(15) Stranges, A. N. In *2003 Spring National Meeting, New Orleans, LA*; 2003; pp. 1–13.

(16) Casci, J. L.; Lok, C. M.; Shannon, M. D. *Catal. Today* **2009**, *145*, 38–44.

(17) Shell website http://www.imagination.com/en/our-work/best-both-worlds-shell.

(18) Stone, F. G. A.; West, R. *Advances in Organometallic Chemistry version, volume 17*; Elsevier Science, 1979.

(19) Schulz, H. *Appl. Catal. A Gen.* **1999**, *186*, 3–12.

(20) Morales, B. Y. F.; Weckhuysen, B. M. *Catalysis* **2006**, *19*, 1–40.

(21) Heriot-Watt University. *BP Statistical Review of World Energy*; 2014; pp. 1–48.

(22) Corbey, D. C. *Biomassa en beleid : hoe sturen op minder CO 2 ? Er is veel onduidelijkheid over de reikwijdte en de doelstelling van de*; 2012; pp. 1–28.

(23) Van Vliet, O. P. R.; Faaij, A. P. C.; Turkenburg, W. C. *Energy Convers. Manag.* **2009**, *50*, 855–876.

(24) Cleveland, C. *Energy* **2005**, *30*, 769–782.

(25) Andrews, A.; Logan, J. *Fischer-Tropsch Fuels from Coal, Natural Gas, and Biomass: Background and Policy*; 2009; p. 30.

(26) De Sa, P. Sustainable Development - Russia, Kazakhstan Lead Way to Reduce Gas Flaring and Lower Emissions.

(27) Van de Loosdrecht, J.; Botes, F. G.; Ciobica, I. M.; Ferreira, A.; Gibson, P.; Moodley, D. J.; Saib, A. M.; Visagie, J. L.; Westrate, C. J.; Niemantsverdriet, J. W. (Hans); Binnemans, K. *Comprehensive Inorganic Chemistry: Fischer-Tropsch Synthesis: Catalysts and Chemistry*; Reedijk, J.; Poeppelmeier, K., Eds.; Oxford: Elsevier, 2013; Vol. 7, pp. 525–557.

(28) Chorkendorff, I.; Niemantsverdriet, J. W. (Hans). *Concepts of Modern Catalysis and Kinetics*; 2nd ed.; Wiley-VCH Verlag GmbH & Co. kGaA: Darmstadt, Germany, 2007; pp. 305–315.

(29) Liu, G.; Larson, E. D.; Williams, R. H.; Kreutz, T. G.; Guo, X. *Energy & Fuels* **2011**, *25*, 415–437.

(30) Dry, M. E. *Appl. Catal. A Gen.* **1996**, *138*, 319–344.

(31) Diehl, F.; Khodakov, A. Y. *Oi* **2009**, *64*, 11–24.

(32) Van Der Laan, G. P.; Beenackers, a. a. C. M. *Catal. Rev.* **1999**, *41*, 255–318.

(33) Iglesia, E. *Appl. Catal. A Gen.* **1997**, *161*, 59–78.

(34) Deugd, R. de; Kapteijn, F.; Moulijn, J. *Top. Catal.* **2003**, *26*, 29–39.

(35) Krishna, R.; Sie, S. T. *Fuel Process. Technol.* **2000**, *64*, 73–105.

(36) Uzuegbunam, F. Chevron's Escravos GTL project finally gets off ground _ BusinessDay.

(37) Den Breejen, J. P.; Radstake, P. B.; Bezemer, G. L.; Bitter, J. H.; Frøseth, V.; Holmen, A.; Jong, K. P. de. *J. Am. Chem. Soc.* **2009**, *131*, 7197–7203.

(38) Boudart, M. *Chem. Rev.* **1995**, *95*, 661–666.

(39) Bezemer, G. L. Cobalt supported on carbon nanofibers as catalysts for the Fischer-Tropsch synthesis, 2006, pp. 1–120.

(40) Riva, R.; Miessner, H.; Vitali, R.; Piero, G. Del. *Appl. Catal. A Gen.* **2000**, *196*, 111–123.

(41) Ma, W.; Jacobs, G.; Keogh, R. a.; Bukur, D. B.; Davis, B. H. *Appl. Catal. A Gen.* **2012**, *437-438*, 1–9.

(42) Vada, S.; Hoff, A.; AdnaneS, E.; Schanke, D.; Holmen, A. *Top. Catal.* **1995**, *2*, 155–162.

(43) Iglesia, E.; Soled, S. L.; Fiato, R. A.; Via, G. H. *J. Catal.* **1993**, *143*, 345–368.

(44) Den Otter, J. H. *Unpublished results*; 2013; p. -.

(45) Van de Loosdrecht, J.; Balzhinimaev, B.; Dalmon, J.-A.; Niemantsverdriet, J. W. (Hans); Tsybulya, S. V.; Saib, A. M.; van Berge, P. J.; Visagie, J. L. *Catal. Today* **2007**, *123*, 293–302.

(46) Tsakoumis, N. E.; Rønning, M.; Borg, Ø.; Rytter, E.; Holmen, A. *Catal. Today* **2010**, *154*, 162–182.

(47) Storsæter, S.; Borg, Ø.; Blekkan, E. A.; Holmen, A. *J. Catal.* **2005**, *231*, 405–419.

(48) Li, J.; Jacobs, G.; Zhang, Y.; Das, T. K.; Davis, B. H.; Racoillet, G. *Appl. Catal. A Gen.* **2002**, *223*, 195–203.

(49) Oukaci, R.; Singleton, A. H.; Goodwin, J. G. *Appl. Catal. A Gen.* **1999**, *186*, 129–144.

(50) Kogelbauer, A.; Goodwin, J. G.; Oukaci, R. *J. Catal.* **1996**, *160*, 125–133.

(51) Van Hardeveld, R.; Hartog, F. *Surf. Sci.* **1969**, *15*, 189–230.

(52) Van Hardeveld, R.; Montfoort, A. van. *Surf. Sci.* **1966**, *4*, 396–430.

(53) Loveless, B. T.; Buda, C.; Neurock, M.; Iglesia, E. *J. Am. Chem. Soc.* **2013**, *135*, 6107–6121.

(54) Cheng, J.; Gong, X.; Hu, P.; Lok, C.; Ellis, P.; French, S. *J. Catal.* **2008**, *254*, 285–295.

(55) Cheng, J.; Hu, P.; Ellis, P.; French, S.; Kelly, G.; Lok, C. *J. Catal.* **2008**, *257*, 221–228.

(56) Den Breejen, J. P. *Cobalt particle size effects in catalysis*; 2010; p. 117.

(57) Breejen, J. Den. *J. …* **2009**, 7197–7203.

(58) Bezemer, G. L.; Bitter, J. H.; Kuipers, H. P. C. E.; Oosterbeek, H.; Holewijn, J. E.; Xu, X.; Kapteijn, F.; van Dillen, A. J.; de Jong, K. P. *J. Am. Chem.* **2006**, *128*, 3956–3964.

(59) Braconnier, L.; Landrivon, E.; Clémençon, I.; Legens, C.; Diehl, F.; Schuurman, Y. *Catal. Today* **2013**, *215*, 18–23.

(60) Ducreux, O.; Rebours, B.; Lynch, J.; Roy-Auberger, M.; Bazin, D. *Oil Gas Sci. Technol.* **2009**, *64*, 49–62.

(61) Karaca, H.; Safonova, O. V.; Chambrey, S.; Fongarland, P.; Roussel, P.; Griboval-Constant, A.; Lacroix, M.; Khodakov, A. Y. *J. Catal.* **2011**, *277*, 14–26.

(62) Jong, K. P. de; Marceau, E.; Carrier, X.; Che, M. In *Synthesis of Heterogeneous catalysts*; 2009.

(63) Eschemann, T. O.; Bitter, J. H.; de Jong, K. P. *Catal. Today* **2013**.

(64) Van Dillen, a. J.; Terörde, R. J. a M.; Lensveld, D. J.; Geus, J. W.; De Jong, K. P. *J. Catal.* **2003**, *216*, 257–264.

(65) Preo, T.; Kallay, N. *Croat. Chem. Acta* **2006**, *79*, 95–106.

(66) Li, J.; Jacobs, G.; Das, T. K.; Davis, B. H. *Appl. Catal. A Gen.* **2002**, *233*, 255–262.

(67) Duvenhage, D.; Coville, N. *Appl. Catal. A Gen.* **1997**.

(68) Storsater, S.; Totdal, B.; Walmsley, J. C.; Tanem, B. S.; Holmen, A. *J. Catal.* **2005**, *236*, 139–152.

(69) Jermwongratanachai, T.; Jacobs, G.; Shafer, W. D.; Pendyala, V. R. R.; Ma, W.; Gnanamani, M. K.; Hopps, S.; Thomas, G. a.; Kitiyanan, B.; Khalid, S.; Davis, B. H. *Catal. Today* **2013**.

(70) Vannice, M. A. *J. Catal.* **1975**, *461*, 449–461.

(71) Fischer, F.; Tropsch, H.; Dilthey, P. *Brennstoff-Chemie* **1925**, *6*, 265.

# Appendix

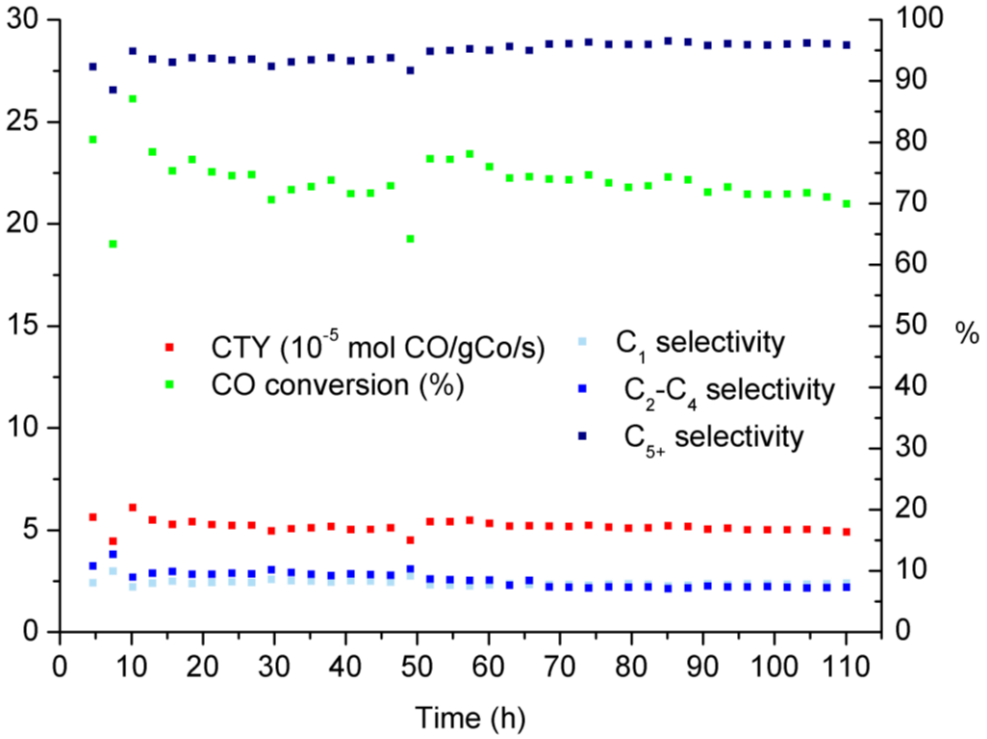


**Figure 18: Data of catalytic run of unpromoted cobalt on titania. On the left y-axis the CTY an CO conversion, while on the right y-axis the methane, C2-C4 and C5+ selectivities are plotted.**

| Catalyst | $d_p$ $H_2$-chem (nm) | $d_p$ XRD (nm) | $X_{CO}$ (%) | CTY ($\cdot 10^{-5}$ mol CO/$g_{Co}$/s) | TOF $H_2$-chem ($s^{-1}$) | TOF XRD ($s^{-1}$) |
|---|---|---|---|---|---|---|
| Co 9,41 | 39,59 | 5,1 | 21,96 | 5,13 | **0,11** | **0,014** |
| Co 9,46 | 30,20 | 10,3 | 29,97 | 7,10 | **0,12** | **0,040** |
| Co 9,20 | 35,84 | 5,9 | 30,86 | 7,53 | **0,15** | **0,025** |
| Co 10,25 | 27,97 | 4,2 | 28,20 | 12,27 | **0,19** | **0,028** |
| Co 9,61 | 68,44 | 3,5 | 26,53 | 6,13 | **0,23** | **0,012** |
| Co 9,21 Ag 0,06 | 25,59 | 6,5 | 30,30 | 10,04 | **0,14** | **0,036** |
| Co 8,98 Ag 0,12 | 24,85 | 5,7 | 33,93 | 11,93 | **0,16** | **0,037** |
| Co 9,9 Ag 0,26 | 27,86 | 4,3 | 33,08 | 10,47 | **0,16** | **0,025** |
| Co 8,83 Ru 0,05 | 27,77 | 5,8 | 20,08 | 7,01 | **0,11** | **0,022** |
| Co 8,00 Ru 0,10 | 19,06 | 4,7 | 40,91 | 15,85 | **0,17** | **0,042** |
| Co 7,27 Ru 0,18 | 15,90 | 6,4 | 31,78 | 13,47 | **0,12** | **0,048** |
| Co 8,85 Pt 0,11 | 17,12 | 4,4 | 30,44 | 10,75 | **0,10** | **0,026** |
| Co 9,05 Pt 0,21 | 17,78 | 6,3 | 59,81 | 20,74 | **0,20** | **0,073** |
| Co 8,22 Pt 0,39 | 16,84 | 3,9 | 34,17 | 13,08 | **0,12** | **0,028** |
| Co 9,58 Re 0,06 | 18,56 | 5,0 | 30,86 | 19,98 | **0,21** | **0,055** |
| Co 9,72 Re 0,13 | 16,56 | 6,2 | 38,99 | 25,02 | **0,23** | **0,086** |
| Co 9,76 Re 0,25 | 13,91 | 4,5 | 39,53 | 25,02 | **0,19** | **0,063** |